Supporting Information

Copper Coordination Chemistry of Sulfur Pendant Cyclen Derivatives: An Attempt to Hinder the Reductive-Induced Demetallation in [64/67]Cu Radiopharmaceuticals

Marianna Tosato[1], Marco Dalla Tiezza[1], Nóra V. May[2], Abdirisak Ahmed Isse[1], Sonia Nardella[1,3], Laura Orian[1], Marco Verona[3], Christian Vaccarin[3], André Alker[4], Helmut Mäcke[5], Paolo Pastore[1], Valerio Di Marco[1,*]

[1] *Department of Chemical Sciences, University of Padova, via Marzolo 1, 35131 Padova, Italy*

[2] *Centre for Structural Science, Research Centre for Natural Sciences, 1117 Magyar Tudósok Körútja 2, Budapest, Hungary*

[3] *Department of Pharmaceutical Sciences, University of Padova, via Marzolo 8, 35131 Padova, Italy*

[4] *Roche Pharmaceutical Research and Early Development, Roche Innovation Center Basel F. Hoffmann-La Roche Ltd, Grenzacherstrasse 124, 4058 Basel, Switzerland*

[5] *Department of Nuclear Medicine, University Hospital Freiburg, Hugstetterstrasse 55, D-79106 Freiburg, Germany*

*Corresponding author: valerio.dimarco@unipd.it

Table S1. Acidity constants (pK_a values) of DO4S, DO3S, DO3SAm, and DO2A2S. The reported uncertainty was obtained by the fitting procedure and represents one standard deviation unit. DOTA and cyclen were also included for comparison purpose.

Ligand	Equilibrium [a]	pK_a
DO4S	$H_3L^{3+} \rightleftharpoons H_2L^{2+} + H^+$	1.9 ± 0.3 [b]
	$H_2L^{2+} \rightleftharpoons HL^+ + H^+$	7.29 [c]
	$HL^+ \rightleftharpoons L + H^+$	10.14 [c]
DO3S	$H_3L^{3+} \rightleftharpoons H_2L^{2+} + H^+$	2.0 ± 0.1 [b]
	$H_2L^{2+} \rightleftharpoons HL^+ + H^+$	7.54 [c]
	$HL^+ \rightleftharpoons L + H^+$	10.86 [c]
DO3SAm	$H_3L^{3+} \rightleftharpoons H_2L^{2+} + H^+$	1.9 ± 0.2 [b]
	$H_2L^{2+} \rightleftharpoons HL^+ + H^+$	7.8 [c]
	$HL^+ \rightleftharpoons L + H^+$	10.42 [c]
DO2A2S	$H_4L^{2+} \rightleftharpoons H_3L^+ + H^+$	1.8 ± 0.1 [b]
	$H_3L^+ \rightleftharpoons H_2L + H^+$	3.44 [c]
	$H_2L \rightleftharpoons HL^- + H^+$	18.30 [c]
	$HL^- \rightleftharpoons L^{2-} + H^+$	
DOTA	$H_6L^{2+} \rightleftharpoons H_5L^+ + H^+$	1.34 [d]
	$H_5L^+ \rightleftharpoons H_4L + H^+$	2.29 [d]
	$H_4L \rightleftharpoons H_3L^- + H^+$	4.63 [e]
	$H_3L^- \rightleftharpoons H_2L^{2-} + H^+$	4.86 [e]
	$H_2L^{2-} \rightleftharpoons HL^{3-} + H^+$	9.18 [e]
	$HL^{3-} \rightleftharpoons L^{4-} + H^+$	11.43 [e]
Cyclen	$H_4L^{4+} \rightleftharpoons H_3L^{3+} + H^+$	0.8 [f]
	$H_3L^{3+} \rightleftharpoons H_2L^{2+} + H^+$	1.6 [f]
	$H_2L^{2+} \rightleftharpoons HL^+ + H^+$	9.51 [c]
	$HL^+ \rightleftharpoons L + H^+$	10.63 [c]

[a] L denotes the ligand in its totally deprotonated form
[b] This work, no ionic strength control
[c] From ref. [1], I = 0.15 mol/L NaNO$_3$, T = 25°C (see reference list at the end of this file)
[d] From ref. [2], I = 0.15 mol/L (NMe$_4$)Cl, T = 25°C
[e] From ref. [3], I = 0.15 mol/L NaCl, T = 25°C
[f] From ref. [4], I = 0.5 mol/L KNO$_3$, T = 25°C

Table S2. Approximate time required to reach equilibrium during the reaction between Cu^{2+} and ligand at various pH. Data were taken from **Figures S4** - **S7**.

pH	Equilibration time				
	DO4S	DO3S	DO3SAm	DO2A2S	DOTA
2.0	~ 10 d	~ 10 d	~ 10 d	~ 4 h	~ 1 h
3.0	~ 20 h	~ 20 h	~ 10 h	~ 10 min	~ 5 min
4.8	~ 50 min	~ 30 min	~ 1 h	< 10 sec	< 10 sec
7.0	< 10 sec	< 10 sec	< 10 sec	< 10 sec	< 10 sec

Table S3. Approximate time required to reach equilibrium during the reaction between Cu^{2+} and ligand at various pH. Higher concentrations than those of **Table S2** were employed for the reactants.

pH	Equilibration time		
	DO4S	DO3S	DO2A2S
2.0 [a]	–	–	~ 20 min
3.0 [b]	~ 2 h	~ 5 h	< 1 min
4.8 [c]	~ 3 min	~ 2 min	< 10 sec
7.0 [d]	< 10 sec	< 10 sec	< 10 sec

[a] pH 2.0: $C_{DO2A2S} = C_{Cu^{2+}} = 1.0 \cdot 10^{-3}$ mol/L
[b] pH 3.0: $C_{DO4S,\ DO3S} = C_{Cu^{2+}} = 9.0 \cdot 10^{-4}$ mol/L; $C_{DO2A2S} = C_{Cu^{2+}} = 8.0 \cdot 10^{-4}$ mol/L
[c] pH 4.8: $C_{DO4S} = C_{Cu^{2+}} = 1.2 \cdot 10^{-3}$ mol/L; $C_{DO3S,\ DO2A2S} = C_{Cu^{2+}} = 1.1 \cdot 10^{-3}$ mol/L
[d] pH 7.0: $C_{DO4S,\ DO3S,\ DO2A2S} = C_{Cu^{2+}} = 1.0 \cdot 10^{-3}$ mol/L

Table S4. UV-Vis spectroscopic data of the Cu^{2+}-ligand complexes.

Ligand	Complex	Transition	λ_{max} (nm)	ε calculated [a] (L/cm·mol)
DO4S	CuL^{2+}	CT	309	$(3.6 \pm 0.9) \cdot 10^3$
		d-d	593	$5.3 \cdot 10^2$ [b]
DO3S	CuL^{2+}	CT	303	$(3.6 \pm 0.2) \cdot 10^3$
		d-d	581	$4.3 \cdot 10^2$ [b]
DO3SAm	CuL^{2+}	CT	304	$(3.7 \pm 0.8) \cdot 10^3$
		d-d	602	$3.2 \cdot 10^2$ [b]
DO2A2S	CuL	CT	272	$(5.0 \pm 0.2) \cdot 10^3$
		d-d	715	$1.6 \cdot 10^2$ [b]
	$CuHL^+$	CT	303	$(4.0 \pm 0.9) \cdot 10^3$
		d-d	680	–

[a]: obtained from the UV-Vis data fitting aimed at the determination of the equilibrium constants.
[b]: estimated from the spectra

Table S5. Electronic and Gibbs free energies (in gas-phase and in water) for the Cyc4Me and DO4S complexes of Cu^{2+}, supposing no sulfur coordination in the latter. All the energies are in kcal/mol. Level of theory: (COSMO-)ZORA-OPBE/TZ2P//ZORA-OPBE/TZP.

Ligand	M	Gas phase		Water	
		ΔE	ΔG	ΔE	ΔG
Cyc4Me	Cu^{2+}	–402.5	–387.1	–198.4	–183.0
DO4S		–412.4	–399.4	–192.7	–179.7

Table S6. Activation Strain Model (ASM) and Energy Decomposition Analysis (EDA) of the DO4S and DO3S complexes of Cu^{2+} and Cu^+. All the energies are in kcal/mol. Level of theory: ZORA-OPBE/TZ2P//ZORA-OPBE/TZP.

M	Ligand	coordination	ΔE	ΔE_{strain}	ΔE_{int}	ΔE_{Pauli}	ΔV_{elstat}	ΔE_{oi}
		[4N]	−412.4	13.7	−426.1	166.5	−234.6	−358.0
	DO4S	[4N,S]	−417.4	21.2	−438.6	142.7	−228.3	−353.0
		[4N,2S]	−410.1	27.3	−437.4	96.6	−198.0	−336.1
Cu^{2+}		[4N]	−411.4	12.4	−423.8	168.2	−241.6	−350.4
	DO3S	[4N,S]	−418.1	21.1	−439.2	153.0	−241.3	−350.9
		[4N,2S]	−411.2	27.8	−439.0	111.0	−214.3	−335.6
		[4N]	−117.3	5.6	−122.9	157.3	−171.1	−109.0
	DO4S	[4N,S]	−128.3	13.7	−142.0	161.0	−179.5	−123.5
		[4N,2S]	−122.5	21.8	−144.3	141.7	−164.9	−121.2
Cu^+		[4N]	−119.7	4.9	−124.5	158.9	−176.3	−107.2
	DO3S	[4N,S]	−130.6	13.4	−144.1	160.3	−182.3	−122.1
		[4N,2S]	−126.2	18.0	−144.2	140.7	−166.4	−118.5

Table S7. Crystallographic data and refinement details for $[Cu(DO4S)(NO_3)] \cdot (NO_3)$.

Empirical formula	$C_{20}H_{44}CuN_6O_6S_4$
Formula weight	656.39 g/mol
Temperature	183 (2)
Radiation and wavelength	Mo-Kα, λ = 0.71073 Å
Crystal system	Monoclinic
Space group	P2 (1)
Unit cell dimension	a = 8.128 Å $\quad$ $α$ = 90.0° $\quad$ b = 14.879 Å $\quad$ $β$ = 102.86° $\quad$ c = 12.373 Å, $\quad$ $γ$ = 90.0°
Volume	1458.8 $Å^3$
Z	2
Density (calculated)	1.494 Mg/cm^3
Absorption coefficient, μ	1.080 mm^{-1}
F(000)	694
Crystal colour	blue
Crystal size	0.6 × 0.4 × 0.4 mm
θ area data collection	1.69 to 27.52°
Index area	$0 ≤ h ≤ 10$, $0 ≤ k ≤ 19$, $−16 ≤ l ≤15$
Reflections collected	3760
Independent reflections	3462 [R(int) = 0.02951]
Refinement method	Full-matrix least squares on F^2
Data/restraints/parameters	3462/1/336
Final R indices [I <2σ(I)]	R_1 = 0.0570, wR_2 = 0.1387
R indices (all data)	R_1 = 0.0736, wR_2 = 0.1527
Absolute structure parameter	0.00 ± 3
Extinction coefficient	0.00 ± 2
Differential signals	0.842 and −0.575 e.$Å^{-3}$

$R_1 = Σ ||F_0|−|F_c||/ Σ |F_0|$

$wR_2 = \{Σ [w(|F_0|^2−|F_c|^2)^2/Σ [w(F_0^4)]\}^{1/2}$

Table S8. Bond lengths of [Cu(DO4S)(NO$_3$)]·(NO$_3$).

Bond	Bond length [Å]	Bond	Bond length [Å]
Cu(1)-N(5)	2.029(7)	S(7)-C(16)	1.773(10)
Cu(1)-N(3)	2.035(7)	S(8)-C(22)	1.784(11)
Cu(1)-N(2)	2.053(7)	S(8)-C(21)	1.805(10)
Cu(1)-N(4)	2.057(7)	S(9)-C(27)	1.690(2)
Cu(1)-O(31)	2.149(6)	S(9)-C(26)	1.799(10)
N(2)-C(13)	1.447(12)	C(10)-C(11)	1.525(11)
N(2)-C(10)	1.469(10)	C(13)-C(14)	1.420(2)
N(2)-C(29)	1.599(13)	C(15)-C(16)	1.518(11)
N(3)-C(18)	1.425(12)	C(18)-C(19)	1.423(14)
N(3)-C(15)	1.477(10)	C(20)-C(21)	1.524(12)
N(3)-C(14)	1.611(12)	C(23)-C(24)	1.453(13)
N(4)-C(23)	1.459(12)	C(25)-C(26)	1.515(13)
N(4)-C(20)	1.482(10)	C(28)-C(29)	1.447(14)
N(4)-C(19)	1.573(12)	N(39)-O(33)	1.168(14)
N(5)-C(28)	1.470(12)	N(30)-O(32)	1.174(14)
N(5)-C(25)	1.482(10)	N(30)-O(31)	1.229(9)
N(5)-C(24)	1.579(13)	N(34)-O(35)	1.194(11)
S(6)-C(12)	1.765(11)	N(34)-O(36)	1.228(12)
S(6)-C(11)	1.811(9)	N(34)-O(37)	1.245(10)
S(7)-C(17)	1.736(14)		

Table S9. Bond angles of [Cu(DO4S)(NO$_3$)]·(NO$_3$).

Angle	[°]	Angle	[°]
N(5)-Cu(1)-N(3)	151.9(3)	C(25)-N(5)-C(24)	110.4(7)
N(5)-Cu(1)-N(2)	86.8(3)	C(28)-N(5)-Cu(1)	101.9(6)
N(3)-Cu(1)-N(2)	86.7(3)	C(25)-N(5)-Cu(1)	114.4(5)
N(5)-Cu(1)-N(4)	87.6(3)	C(24)-N(5)-Cu(1)	103.3(5)
N(3)-Cu(1)-N(4)	84.8(3)	C(12)-S(6)-C(11)	101.4(5)
N(2)-Cu(1)-N(4)	150.7(3)	C(17)-S(7)-C(16)	102.1(8)
N(5)-Cu(1)-O(31)	104.6(3)	C(22)-S(8)-C(21)	100.9(8)
N(3)-Cu(1)-O(31)	103.3(3)	C(27)-S(9)-C(26)	99.7(8)
N8")-Cu(1)-O(31)	110.5(3)	N(2)-C(10)-C(11)	114.2(6)
N(4)-Cu(1)-O(31)	98.7(3)	C(10)-C(11)-S(6)	109.8(6)
C(13)-N(2)-C(10)	115.8(7)	C(14)-C(13)-N(2)	108.4(8)
C(13)-N(2)-C(29)	110.9(8)	C(13)-C(14)-N(3)	111.0(8)
C(10)-N(2)-C(29)	108.8(7)	N(3)-C(15)-C(16)	115.6(6)
C(13)-N(2)-Cu(1)	102.0(6)	C(15)-C(16)-S(7)	111.9(6)
C(10)-N(2)-Cu(1)	115.4(5)	C(19)-C(18)-N(3)	108.2(8)
C(29)-N(2)-Cu(1)	103.1(5)	C(18)-C(19)-N(4)	111.2(7)
C(18)-N(3)-C(15)	116.6(7)	N(4)-C(20)-C(21)	114.2(7)
C(18)-N(3)-C(14)	109.2(7)	C(20)-C(21)-S(8)	109.2(6)
C(15)-N(3)-C(14)	108.8(7)	C(24)-C(23)-N(4)	108.8(7)
C(18)-N(3)-Cu(1)	102.7(6)	C(23)-C(24)-N(5)	110.9(7)
C(15)-N(3)-Cu(1)	116.0(4)	N(5)-C(25)-C(26)	114.2(7)
C(14)-N(3)-Cu(1)	102.6(5)	C(25)-C(26)-S(9)	112.1(7)
C(23)-N(4)-C(20)	114-1(7)	C(29)-C(28)-N(5)	110.5(9)
C(23)-N(4)-C(19)	111.2(7)	O(33)-N(30)-O(32)	120.6(12)
C(20)-N(4)-C(19)	110.7(7)	O(33)-N(30)-O(31)	118.2(11)
C(23)-N(4)-Cu(1)	101.1(5)	O(32)-N(30)-O(31)	120.0(11)
C(20)-N(4)-Cu(1)	115.3(5)	N(30)-O(31)-Cu(1)	136.1(5)
C(19)-N(4)-Cu(1)	103.5(5)	O(35)-N(34)-O(36)	120.0(9)
C(28)-N(5)-C(25)	115.4(8)	O(35)-N(34)-O(37)	120.2(9)
C(28)-N(5)-C(24)	110.5(7)	O(36)-N(34)-O(37)	119.7(8)

Table S10. Crystal data and structure refinement for [Cu(DO2A2S)].

Empirical formula	$C_{18}H_{34}CuN_4O_4S_2$
Formula weight	498.15
Temperature	295(2)
Radiation and wavelength	Mo-Kα, λ =0.71073 Å
Crystal system	monoclinic
Space group	I 2
Unit cell dimensions	a = 16.1921(10) Å $\quad$ α = 90.0°
	b = 6.7295(4) Å $\quad$ β = 91.554(10)°
	c = 19.970(3) Å, $\quad$ γ = 90.0°
Volume	2175.2(4) Å^3
Z/Z'	4/1
Density (calculated)	1.521 Mg/m^3
Absorption coefficient, μ	1.228 mm^{-1}
F(000)	1052
Crystal colour	blue
Crystal description	block
Crystal size	0.30 × 0.30 × 0.20 mm
Absorption correction	numerical
Max. and min. transmission	0.928, 0.966
θ range for data collection	3.195 $\leq \theta \leq$ 27.468°
Index ranges	$-20 \leq h \leq 20$; $-8 \leq k \leq 8$; $-25 \leq l \leq 25$
Reflections collected	23317
Completeness to 2θ	0.998
Independent reflections	4964 [R(int) = 0.0421]
Reflections $I>2\sigma(I)$	4599
Refinement method	full-matrix least-squares on F^2
Data / restraints / parameters	4964 /1 /266
Goodness-of-fit on F^2	1.038
Final R indices [$I>2\sigma(I)$]	R_1 = 0.0298, wR_2 = 0.0616
R indices (all data)	R_1 = 0.0345, wR_2 = 0.0628
Max. and mean shift/esd	0.000; 0.000
Largest diff. peak and hole	0.396; -0.202 e.Å^{-3}

Table S11. Bond lengths for [Cu(DO2A2S)].

Bond	Bond length [Å]	Bond	Bond length [Å]
Cu1-O1#1	1.954(2)	Cu1-O1	1.955(2)
Cu1-N1#1	2.150(3)	Cu1-N1	2.150(3)
S1-C9	1.789(4)	S1-C8	1.813(3)
O1-C6	1.283(4)	O2-C6	1.231(4)
N1-C5	1.481(4)	N1-C3	1.482(4)
N1-C4#1	1.490(4)	N2-C2	1.461(4)
N2-C1	1.476(4)	N2-C7	1.478(4)
C1-C4	1.514(4)	C2-C3	1.521(5)
C5-C6	1.510(5)	C7-C8	1.515(5)
Cu2-O3#2	1.955(2)	Cu2-O3	1.955(2)
Cu2-N3#2	2.110(3)	Cu2-N3	2.110(3)
Cu2-N4#2	2.336(3)	Cu2-N4	2.336(3)
S2-C19	1.785(4)	S2-C18	1.812(4)
O3-C16	1.277(4)	O4-C16	1.229(4)
N3-C15	1.485(4)	N3-C12	1.489(4)
N3-C11	1.490(4)	N4-C14	1.463(4)
N4-C13	1.479(4)	N4-C17	1.489(4)
C11-C14#2	1.523(4)	C12-C13	1.528(5)
C15-C16	1.526(5)	C17-C18	1.521(4)

Table S12. Bond angles for [Cu(DO2A2S)].

Angle	[°]	Angle	[°]
O1#1-Cu1-O1	87.0(1)	O1#1-Cu1-N1#1	80.3(1)
O1-Cu1-N1#1	157.49(9)	O1#1-Cu1-N1	157.49(9)
O1-Cu1-N1	80.3(1)	N1#1-Cu1-N1	117.2(2)
C9-S1-C8	101.2(2)	C6-O1-Cu1	118.0(2)
C5-N1-C3	110.3(2)	C5-N1-C4#1	107.1(3)
C3-N1-C4#1	110.8(3)	C5-N1-Cu1	102.5(2)
C3-N1-Cu1	114.5(2)	C4#1-N1-Cu1	111.1(2)
C2-N2-C1	109.9(2)	C2-N2-C7	111.4(2)
C1-N2-C7	110.1(2)	N2-C1-C4	111.1(2)
N2-C2-C3	110.9(2)	N1-C3-C2	111.6(3)
N1#1-C4-C1	112.0(3)	N1-C5-C6	110.4(2)
O2-C6-O1	125.3(3)	O2-C6-C5	119.6(3)
O1-C6-C5	115.1(3)	N2-C7-C8	112.5(3)
C7-C8-S1	112.9(2)	O3#2-Cu2-O3	89.6(1)
O3#2-Cu2-N3#2	84.1(1)	O3-Cu2-N3#2	169.4(1)
O3#2-Cu2-N3	169.4(1)	O3-Cu2-N3	84.1(1)
N3#2-Cu2-N3	103.3(2)	O3#2-Cu2-N4#2	107.21(9)
O3-Cu2-N4#2	94.2(1)	N3#2-Cu2-N4#2	79.70(9)
N3-Cu2-N4#2	81.75(9)	O3#2-Cu2-N4	94.2(1)
O3-Cu2-N4	107.21(9)	N3#2-Cu2-N4	81.75(9)
N3-Cu2-N4	79.70(9)	N4#2-Cu2-N4	149.9(1)
C19-S2-C18	102.2(2)	C16-O3-Cu2	117.2(2)
C15-N3-C12	111.2(2)	C15-N3-C11	111.2(3)
C12-N3-C11	110.4(3)	C15-N3-Cu2	104.3(2)
C12-N3-Cu2	109.7(2)	C11-N3-Cu2	109.8(2)
C14-N4-C13	114.6(3)	C14-N4-C17	113.2(3)
C13-N4-C17	112.5(2)	C14-N4-Cu2	101.4(2)
C13-N4-Cu2	107.6(2)	C17-N4-Cu2	106.5(2)
N3-C11-C14#2	111.3(2)	N3-C12-C13	112.0(3)
N4-C13-C12	113.4(2)	N4-C14-C11#2	111.4(2)
N3-C15-C16	113.7(3)	O4-C16-O3	125.8(4)
O4-C16-C15	118.1(3)	O3-C16-C15	116.0(3)
N4-C17-C18	115.2(3)	C17-C18-S2	111.1(2)

Symmetry codes to generate equivalent atoms: #1 –x+1,y,–z+1 and #2 –x+2,y,–z+1

Table S13. ^{1}H-NMR resonance assignments for the Cu$^+$ complexes formed by DO4S and DO2A2S (400 MHz, RT, H_2O + 10% D_2O).

Complex	Signal (ppm)	Multiplicity	Area	Proton Assignation
Cu$^+$-DO4S	2.20	s	12	SCH$_3$
	2.72	s broad	16	SCH$_2$ + NCH$_2$ arms or NCH$_2$ ring
	2.82	s broad	16	NCH$_2$ ring or SCH$_2$ + NCH$_2$ arms
Cu$^+$-DO2A2S	2.28	s	6	SCH$_3$
	2.71	m	4	SCH$_2$
	2.80	t	8	NCH$_2$ ring
	2.92	m	4	NCH$_2$
	2.94	t	8	NCH$_2$ ring
	3.41	s	4	CH$_2$COOH
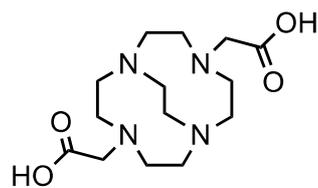
CB-DO2A
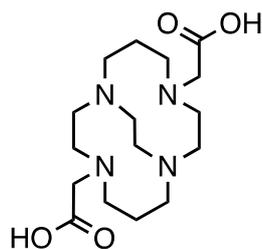
CB-TE2A
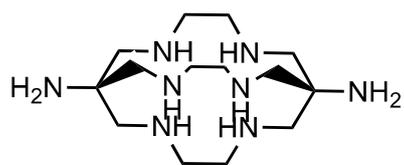
DiamSar

Figure S1. CB-DO2A, CB-TE2A and DiamSar.
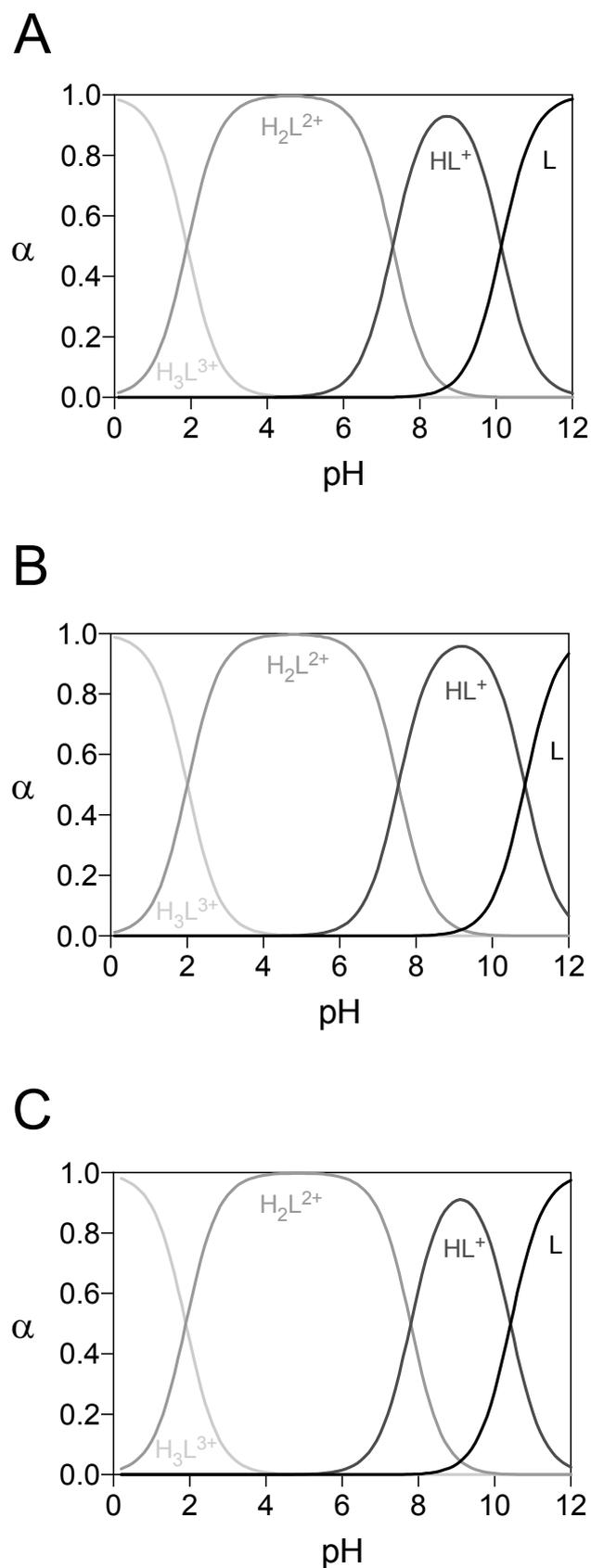
Figure S2. Distribution diagram of (A) DO4S, (B) DO3S and (C) DO3SAm, calculated using the protonation constants listed in **Table S1**.
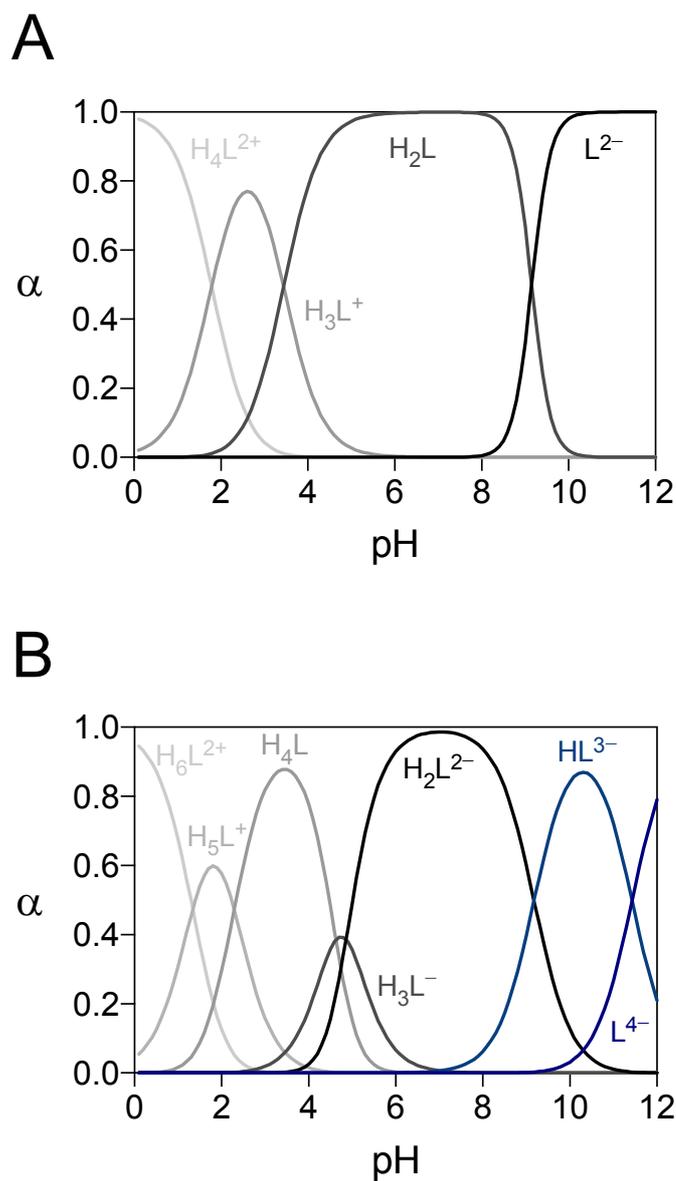
Figure S3. Distribution diagram of (A) DO2A2S and (B) DOTA calculated using the protonation constants listed in **Table S1**.
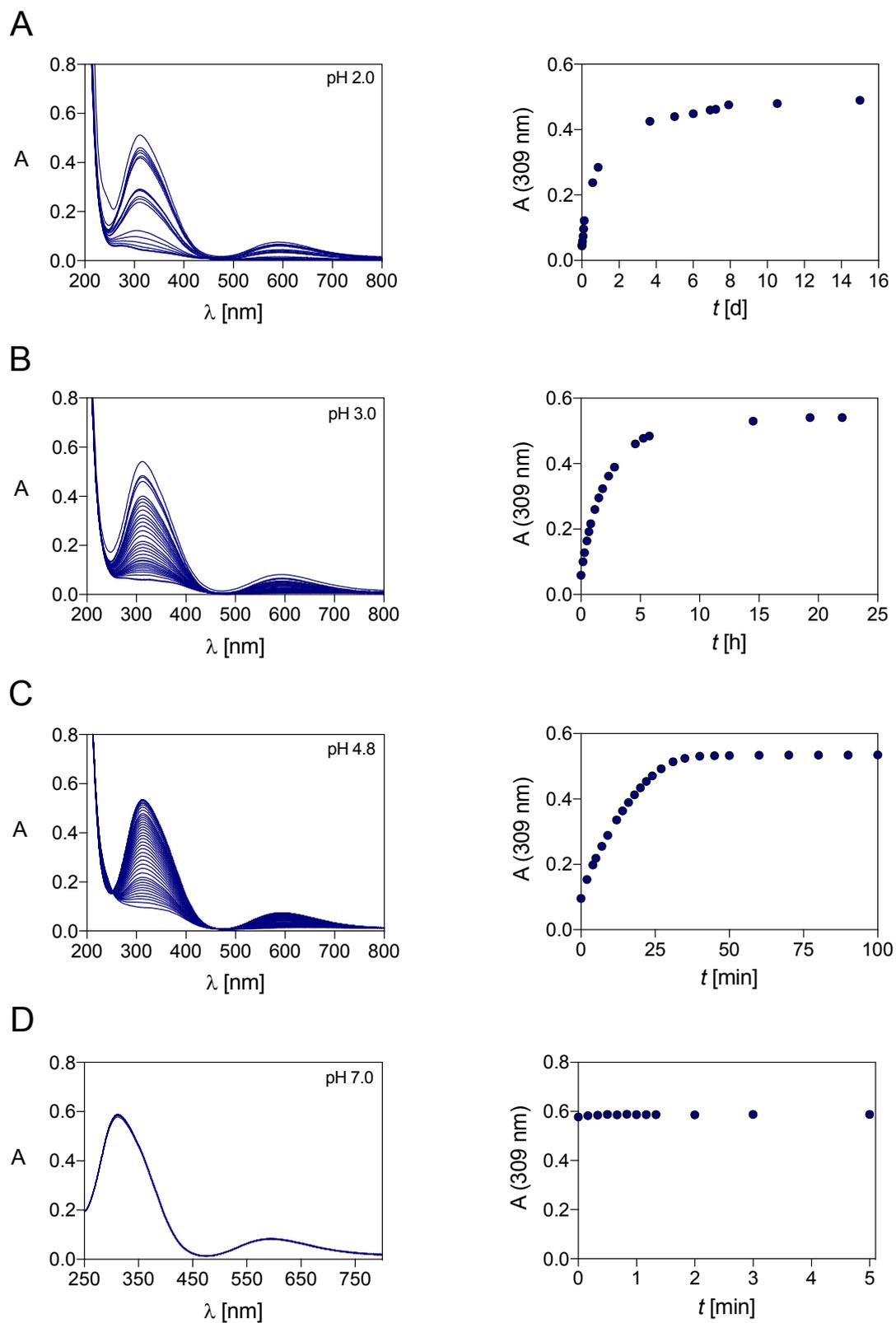
Figure S4. UV-Vis spectra (left) and time course (right) of the Cu^{2+}-DO4S complex formation at (A) pH 2.0 ($C_{DO4S} = C_{Cu^{2+}} = 1.2 \cdot 10^{-4}$ mol/L), (B) pH 3.0 ($C_{DO4S} = C_{Cu^{2+}} = 1.5 \cdot 10^{-4}$ mol/L), (C) pH 4.8 ($C_{DO4S} = C_{Cu^{2+}} = 1.3 \cdot 10^{-4}$ mol/L) and (D) pH 7.0 ($C_{DO4S} = C_{Cu^{2+}} = 1.5 \cdot 10^{-4}$ mol/L).
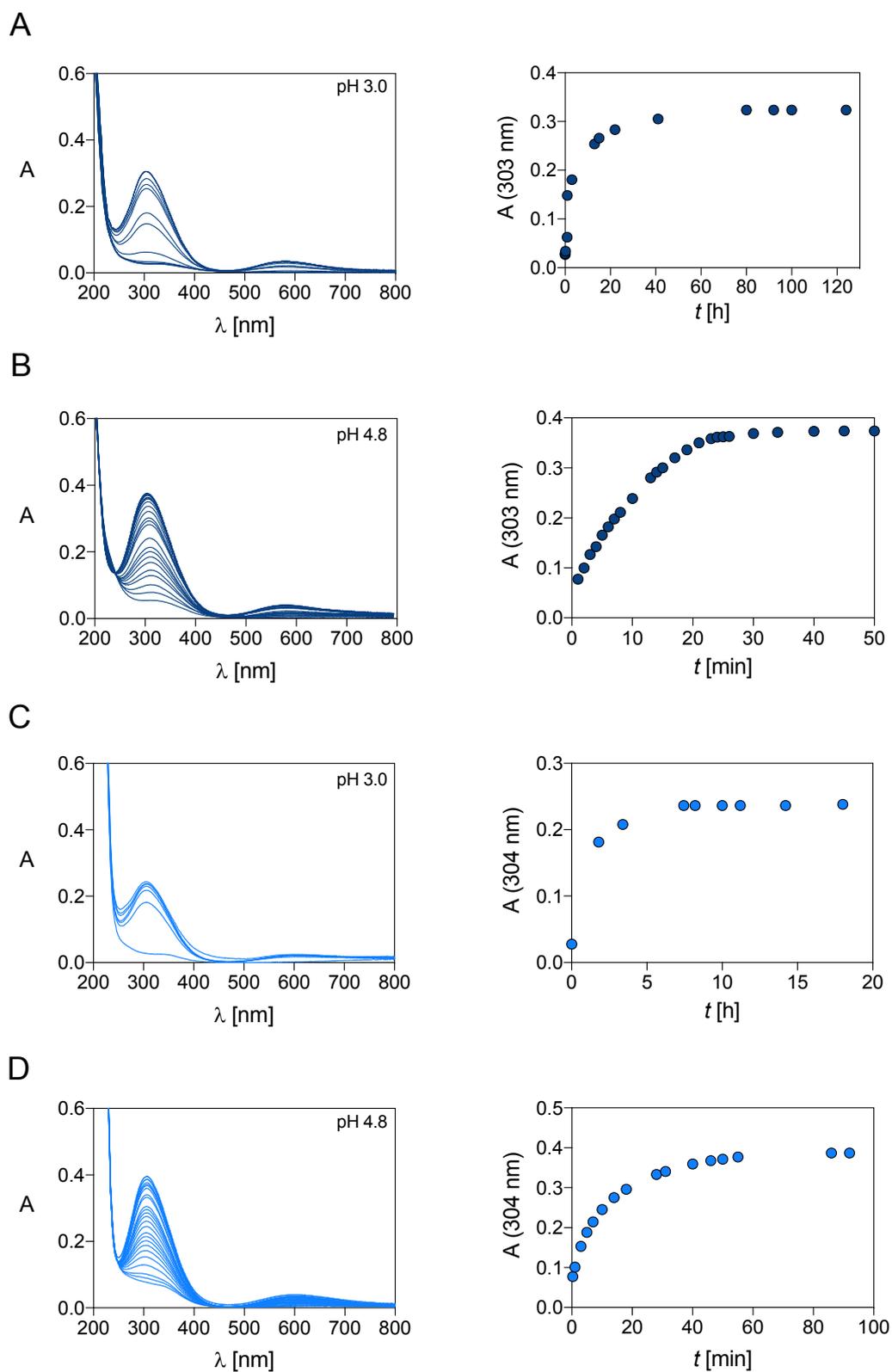
Figure S5. UV-Vis spectra (left) and time course (right) of the Cu^{2+} complex formation with: (A) DO3S at pH 3.0 ($C_{DO3S} = C_{Cu^{2+}} = 1.0 \cdot 10^{-4}$ mol/L); (B) DO3S at pH 4.8 ($C_{DO3S} = C_{Cu^{2+}} = 1.2 \cdot 10^{-4}$ mol/L); (C) DO3SAm at pH 3.0 ($C_{DO3SAm} = C_{Cu^{2+}} = 0.8 \cdot 10^{-4}$ mol/L); (D) DO3SAm at pH 4.8 ($C_{DO3SAm} = C_{Cu^{2+}} = 1.1 \cdot 10^{-4}$ mol/L).
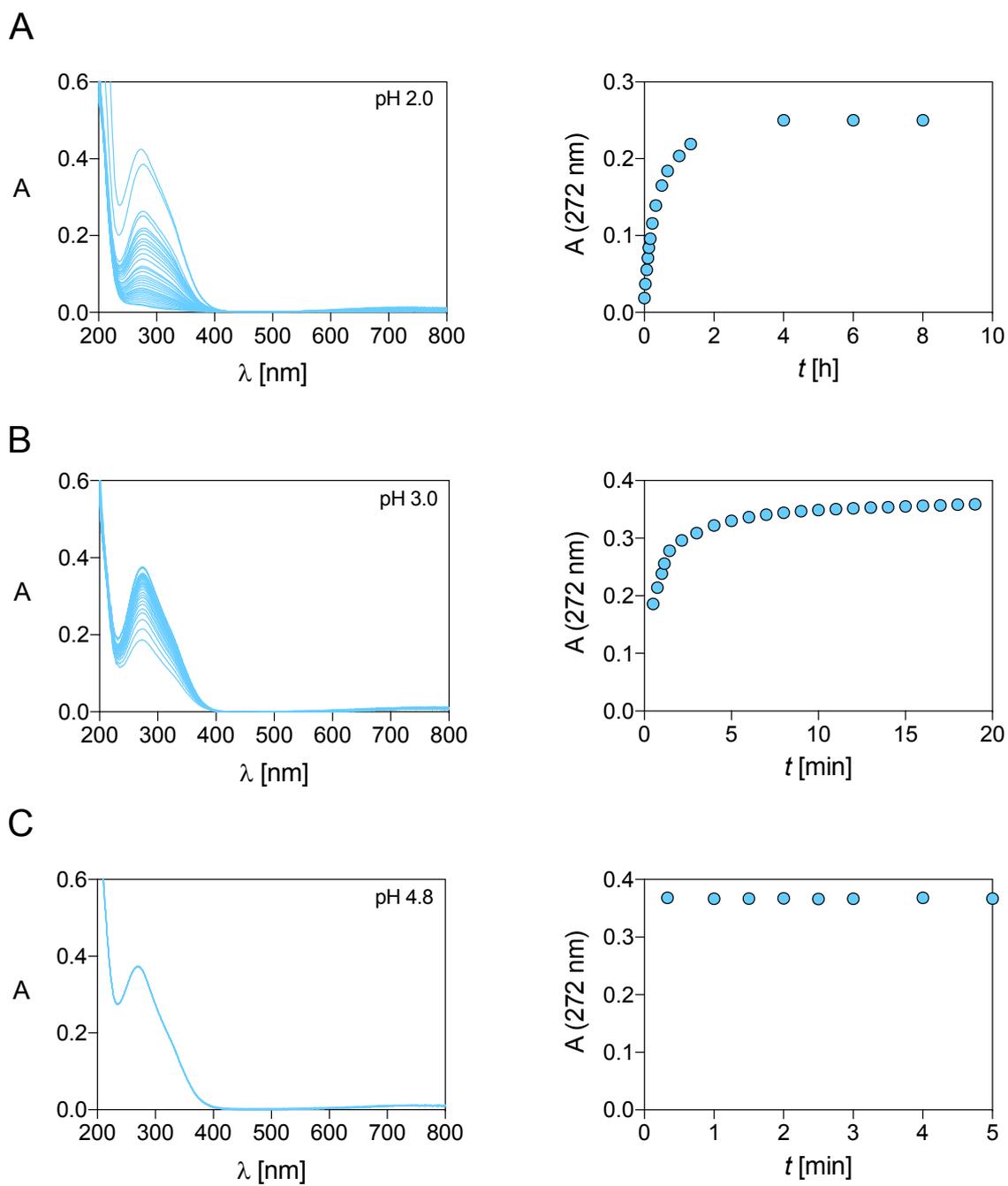
Figure S6. UV-Vis spectra (left) and time course (right) of the Cu^{2+}-DO2A2S complex formation at (A) pH 2.0 ($C_{DO2A2S} = C_{Cu^{2+}} = 0.8 \cdot 10^{-4}$ mol/L), (B) pH 3.0 ($C_{DO2A2S} = C_{Cu^{2+}} = 0.8 \cdot 10^{-4}$ mol/L) and (C) pH 4.8 ($C_{DO2A2S} = C_{Cu^{2+}} = 1.1 \cdot 10^{-4}$ mol/L).

A

B

C
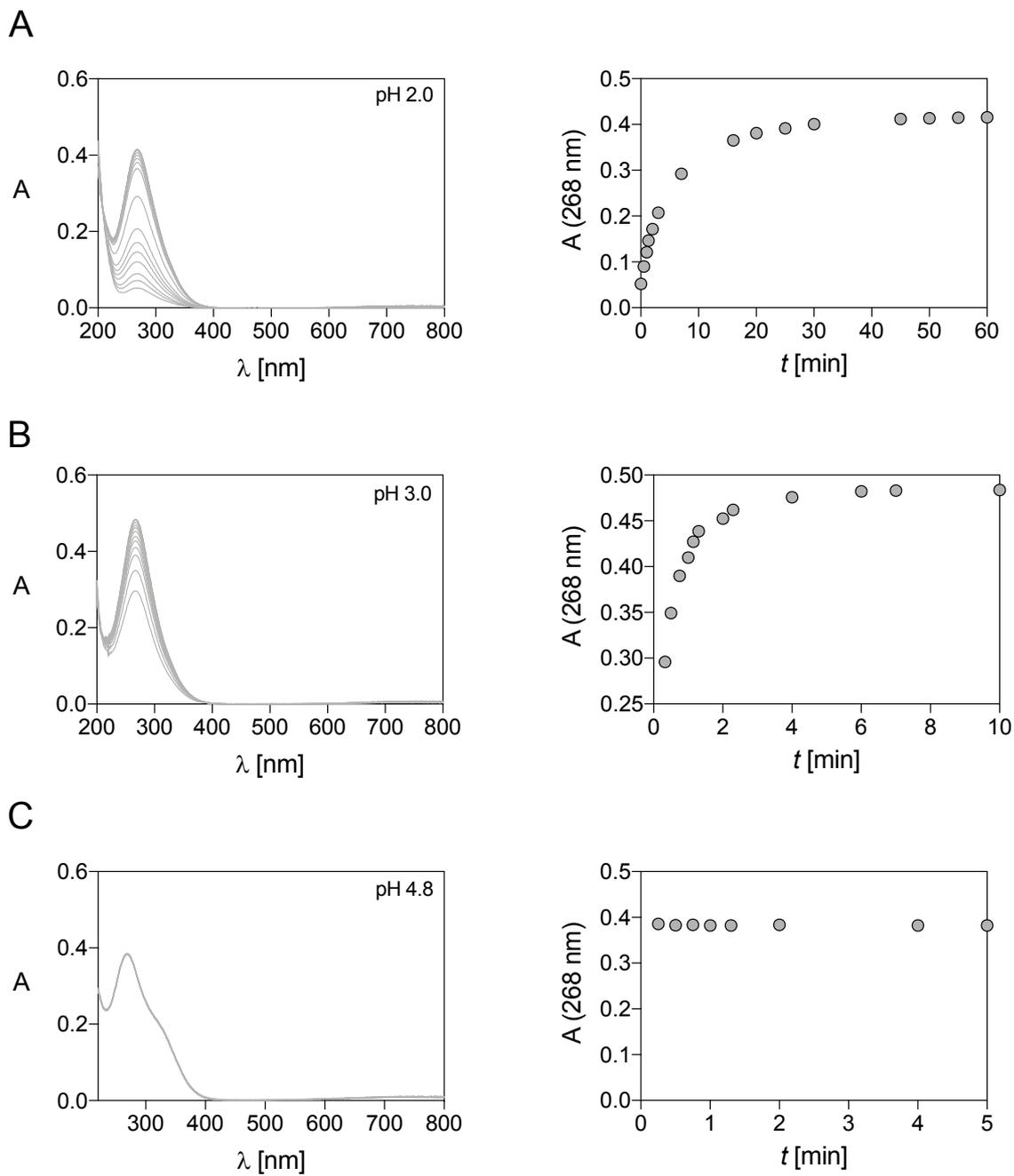
Figure S7. UV-Vis spectra (left) and time course (right) of the Cu^{2+}-DOTA complex formation at (A) pH 2.0 ($C_{DOTA} = C_{Cu^{2+}} = 1.0 \cdot 10^{-4}$ mol/L), (B) pH 3.0 ($C_{DOTA} = C_{Cu^{2+}} = 1.0 \cdot 10^{-4}$ mol/L) and (C) pH 4.8 ($C_{DOTA} = C_{Cu^{2+}} = 1.0 \cdot 10^{-4}$ mol/L).
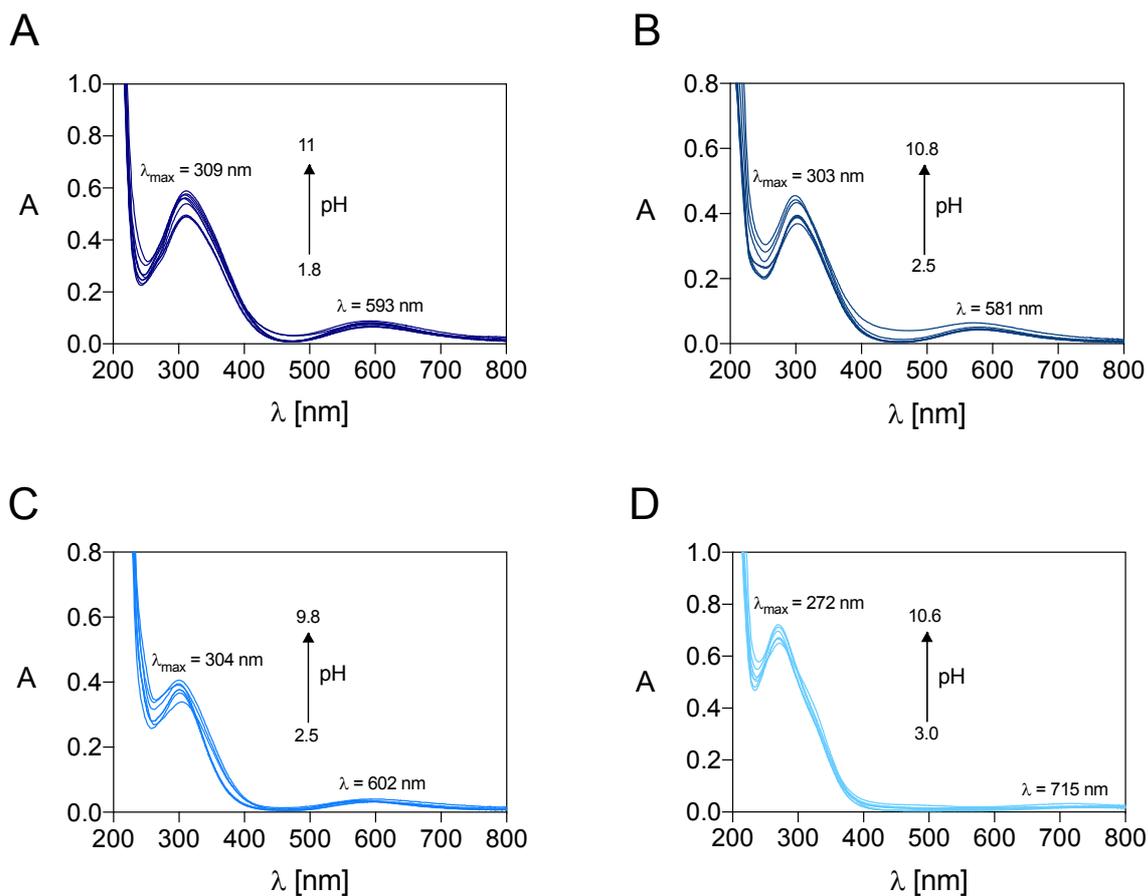
Figure S8. Selected UV-Vis spectra at pH > 2 of the Cu^{2+} complexes with (A) DO4S ($C_{Cu^{2+}}$ = C_{DO4S} = 1.5·10^{-4} mol/L), (B) DO3S ($C_{Cu^{2+}}$ = C_{DO3S} = 1.1·10^{-4} mol/L), (C) DO3SAm ($C_{Cu^{2+}}$ = C_{DO3SAm} = 1.0·10^{-4} mol/L) and (D) DO2A2S ($C_{Cu^{2+}}$ = C_{DO2A2S} = 1.4·10^{-4} mol/L) at I = 0.15 mol/L NaCl and T = 25.0°C.
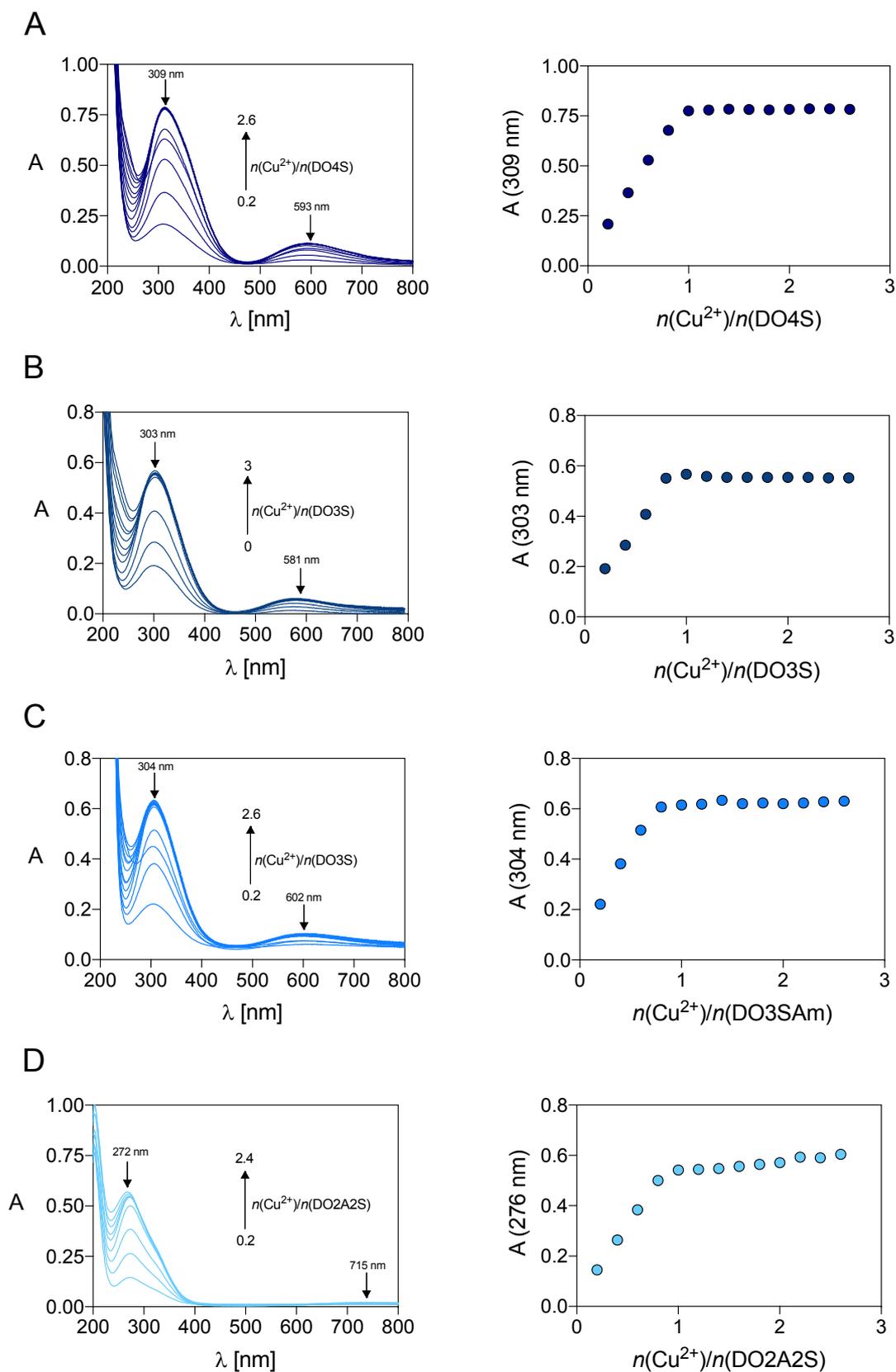
Figure S9. UV-Vis titrations by Cu^{2+} of solutions at pH 4.8 containing (A) DO4S (C_{DO4S} = 2.0·10^{-4} mol/L), (B) DO3S (C_{DO3S} = 1.6·10^{-4} mol/L), (C) DO3SAm (C_{DO3SAm} = 1.6·10^{-4} mol/L) and (D) DO2A2S (C_{DO2A2S} = 1.2·10^{-4} mol/L).
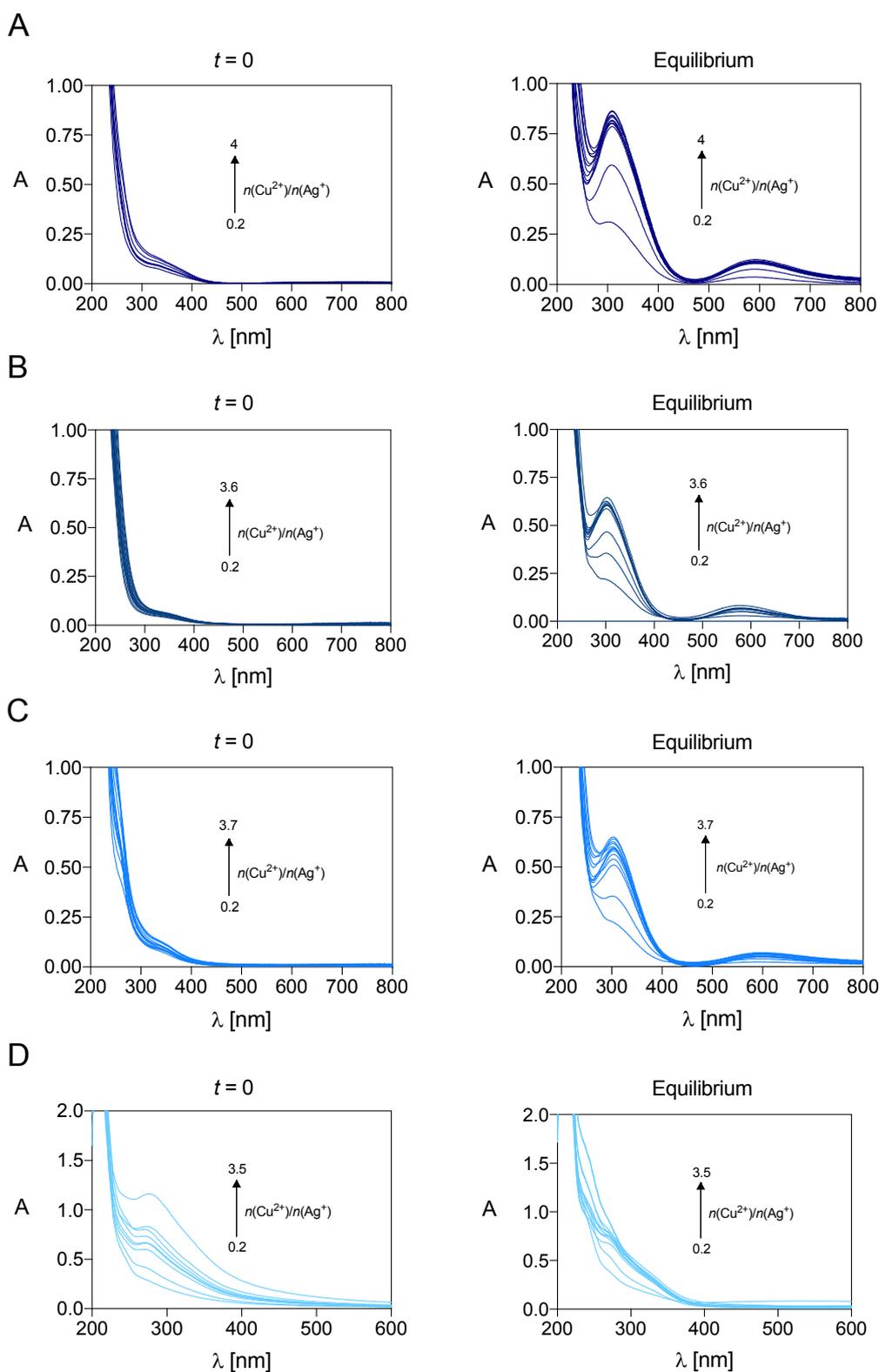
Figure S10. UV-Vis spectra at pH 4.8 of the preformed Ag$^+$ complex with (A) DO4S (C_{Ag^+} = C_{DO4S} = 2.2·10^{-4} mol/L), (B) DO3S (C_{Ag^+} = C_{DO3S} = 1.5·10^{-4} mol/L), (C) DO3SAm (C_{Ag^+} = C_{DO4S} = 1.6·10^{-4} mol/L) and (D) DO2A2S (C_{Ag^+} = C_{DO4S} = 1.2·10^{-4} mol/L) immediately after the addition of variable equivalents of Cu^{2+} (t = 0) and at equilibrium during the competition titrations.
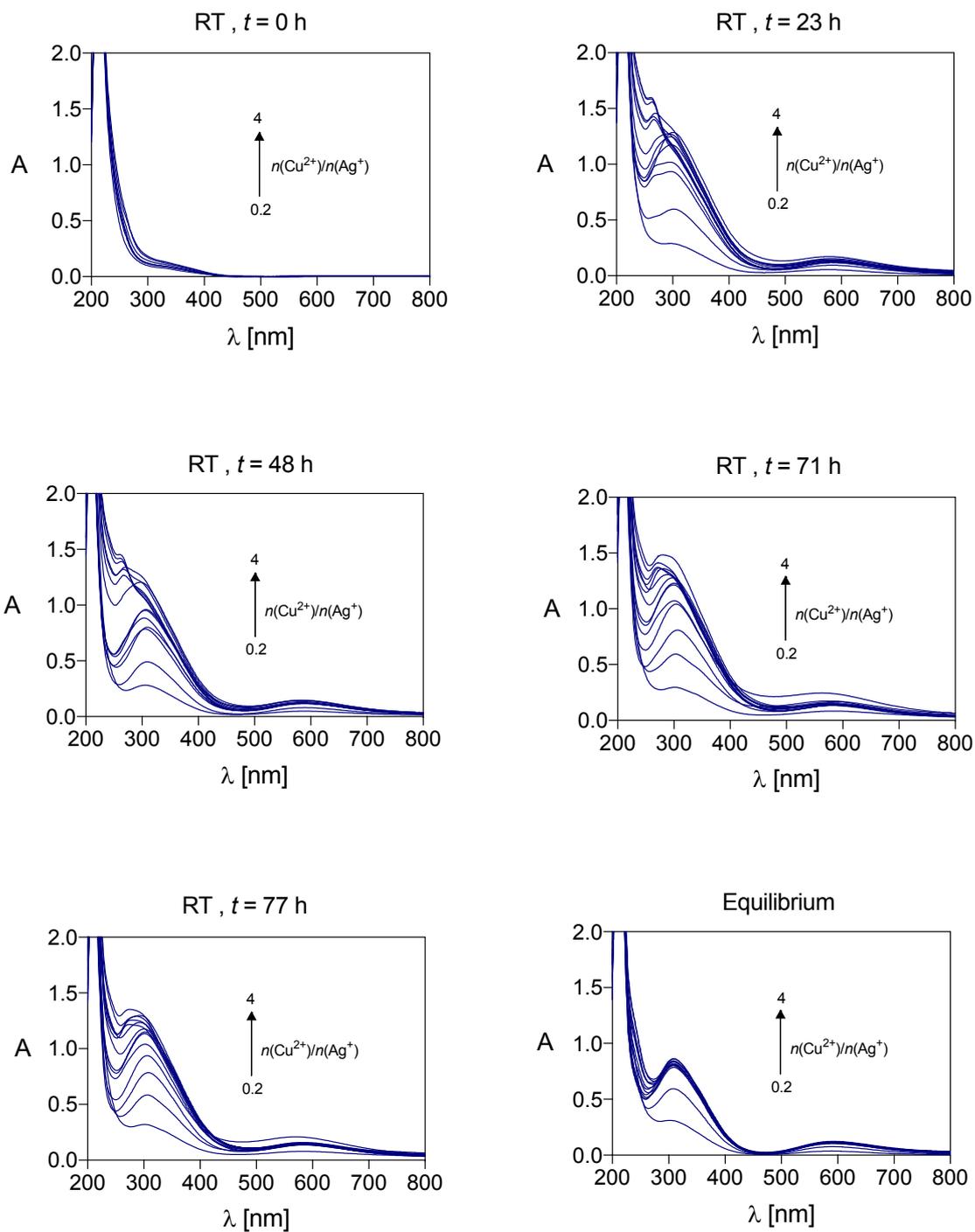
Figure S11. Changes in the UV-Vis spectra over time at pH 4.8 of the preformed Ag⁺ complex with DO4S ($C_{Ag^+} = C_{DO4S} = 2.2 \cdot 10^{-4}$ mol/L) during the Cu²⁺ competition titrations.
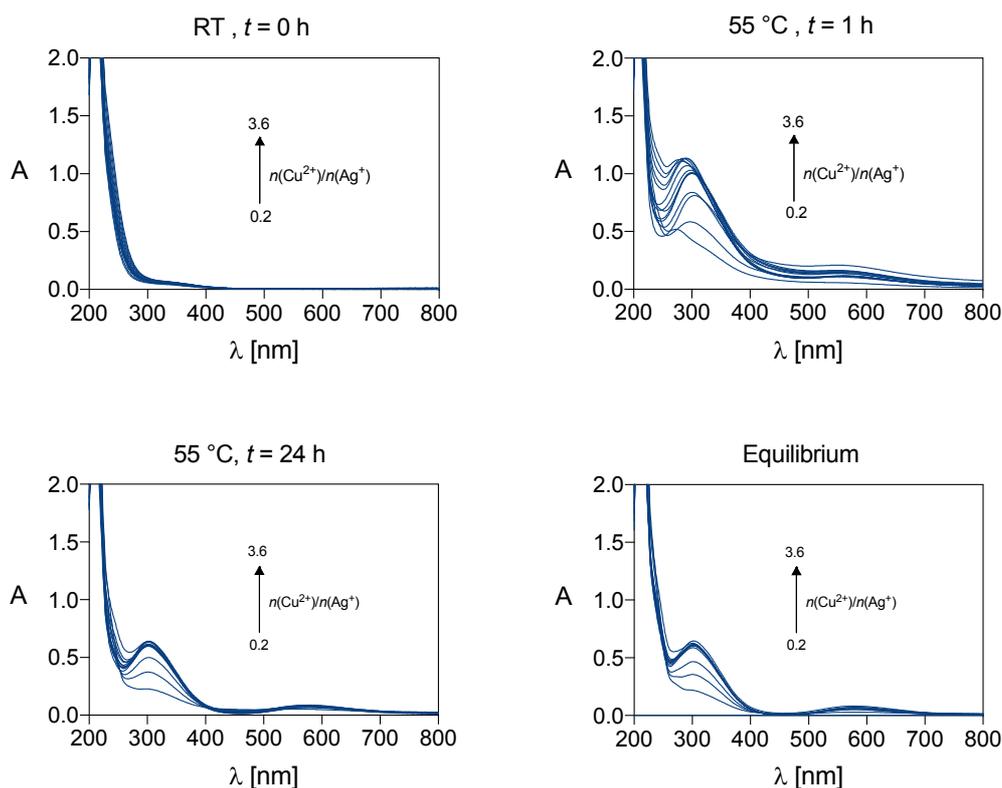
Figure S12. Changes in the UV-Vis spectra over time at pH 4.8 of the preformed Ag$^+$ complex with DO3S (C_{Ag^+} = C_{DO3S} = 1.5·10^{-4} mol/L) during the Cu^{2+} competition titrations.
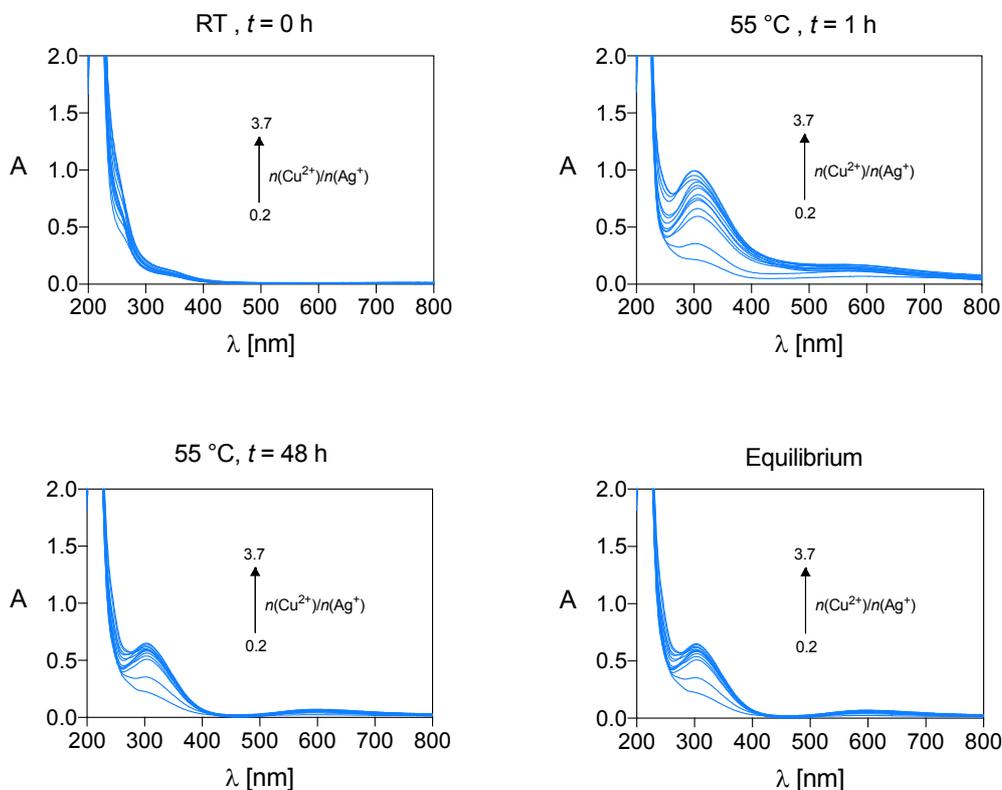
Figure S13. Changes in the UV-Vis spectra over time at pH 4.8 of the preformed Ag$^+$ complex with DO3SAm (C_{Ag^+} = C_{DO3SAm} = 1.6·10^{-4} mol/L) during the Cu^{2+} competition titrations.
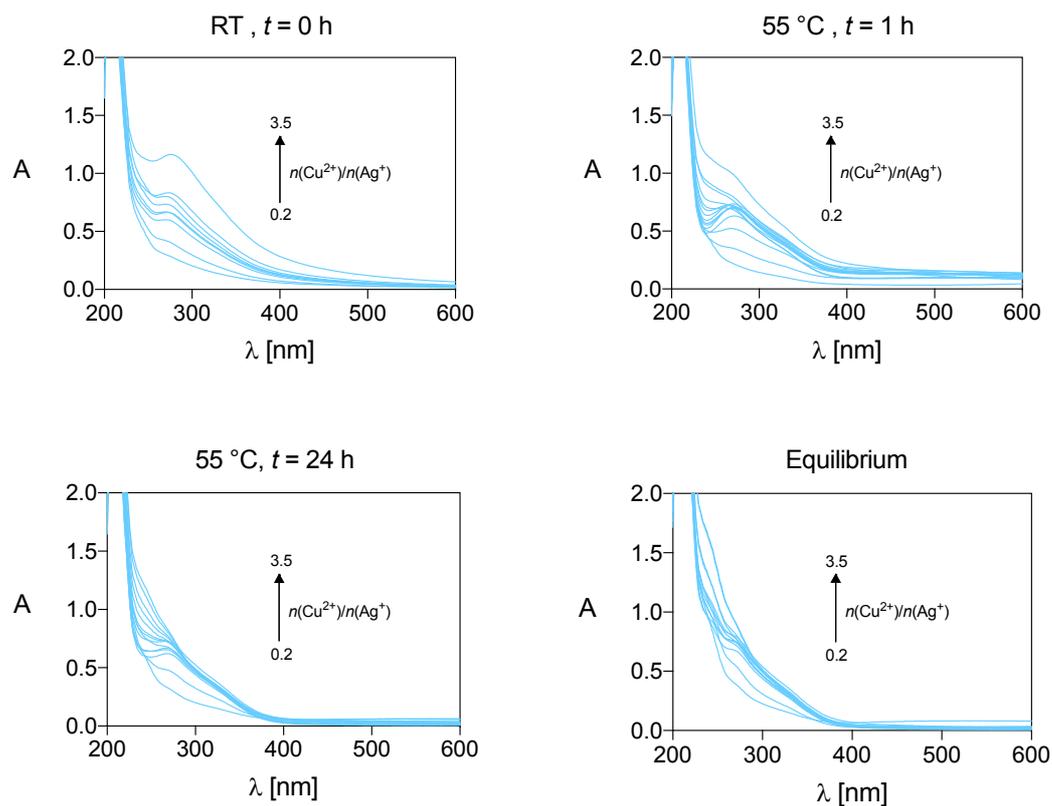
Figure S14. Changes in the UV-Vis spectra over time at pH 4.8 of the preformed Ag$^+$ complex with DO2A2S (C_{Ag^+} = C_{DO2A2S} = 1.2·10^{-4} mol/L) during the Cu^{2+} competition titrations.
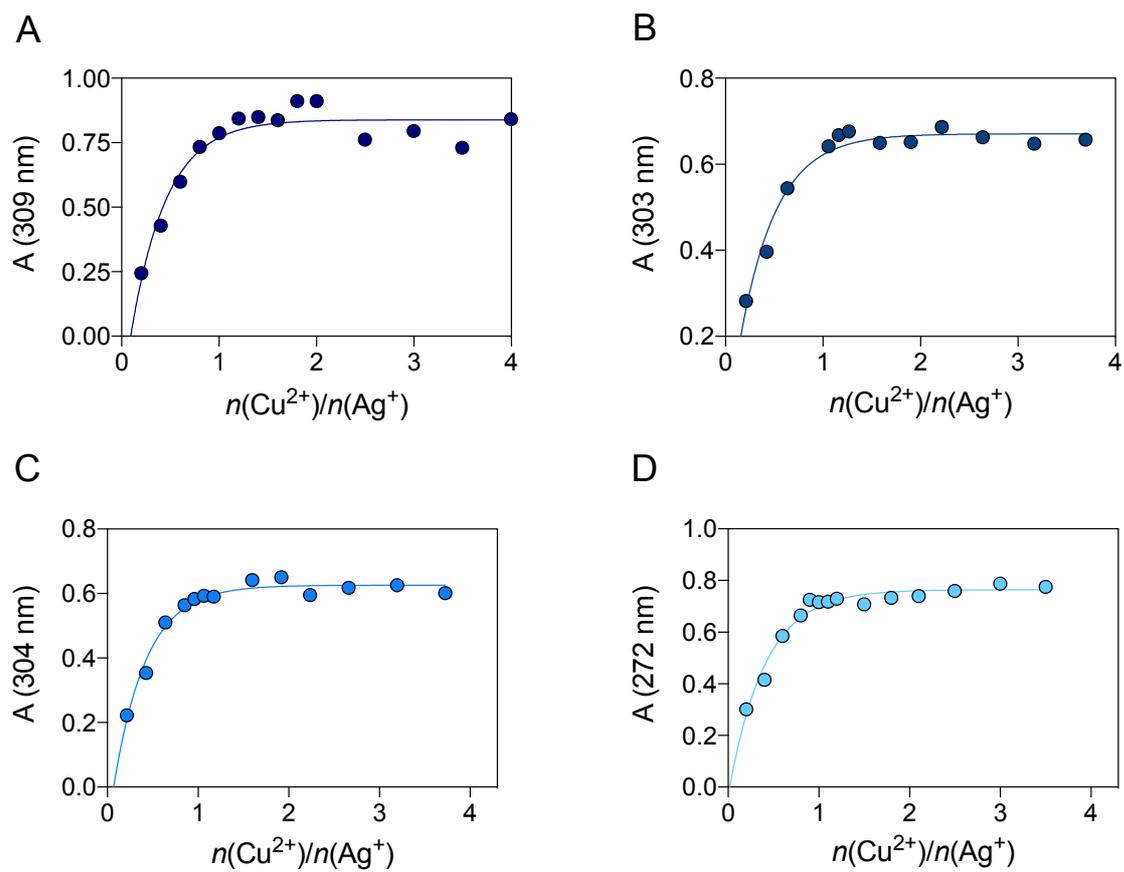
Figure S15. Representative *A* vs. $n(Cu^{2+})/n(Ag^+)$ profiles obtained during the Ag^+-Cu^{2+} competitions measurements (see **Figure S10**) and corresponding fitting lines.
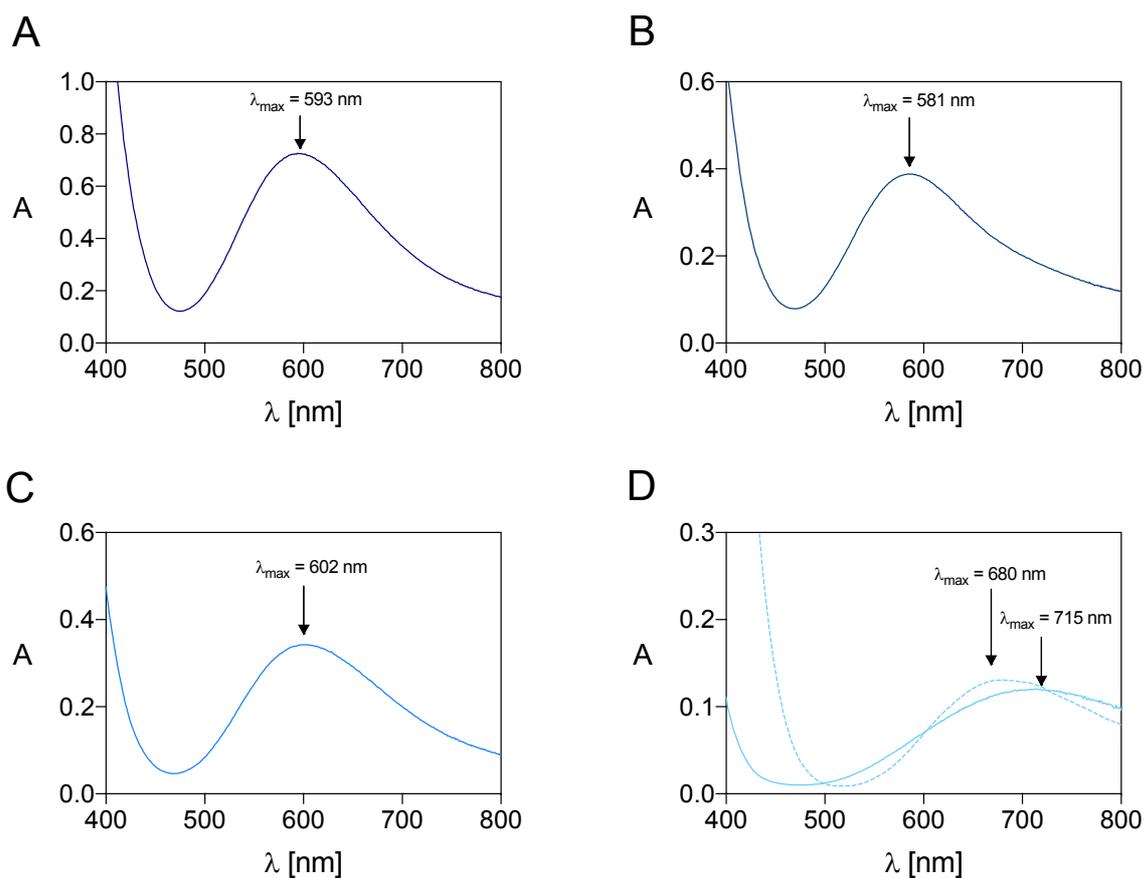
Figure S16. *d-d* band of the cupric complexes with (A) DO4S ($C_{Cu^{2+}}$ = C_{DO4S} = 1.2·10^{-3} mol/L), (B) DO3S ($C_{Cu^{2+}}$ = C_{DO3S} = 9.2·10^{-4} mol/L), (C) DO3SAm ($C_{Cu^{2+}}$ = C_{DO3SAm} = 1.1·10^{-3} mol/L) and (D) DO2A2S (pH 2.0, $C_{Cu^{2+}}$ = C_{DO2A2S} = 7.8·10^{-4} mol/L; pH 1.8 (dotted line), $C_{Cu^{2+}}$ = C_{DO2A2S} = 9.0·10^{-4} mol/L) at *I* = 0.15 mol/L NaCl and *T* = 25.0 °C.
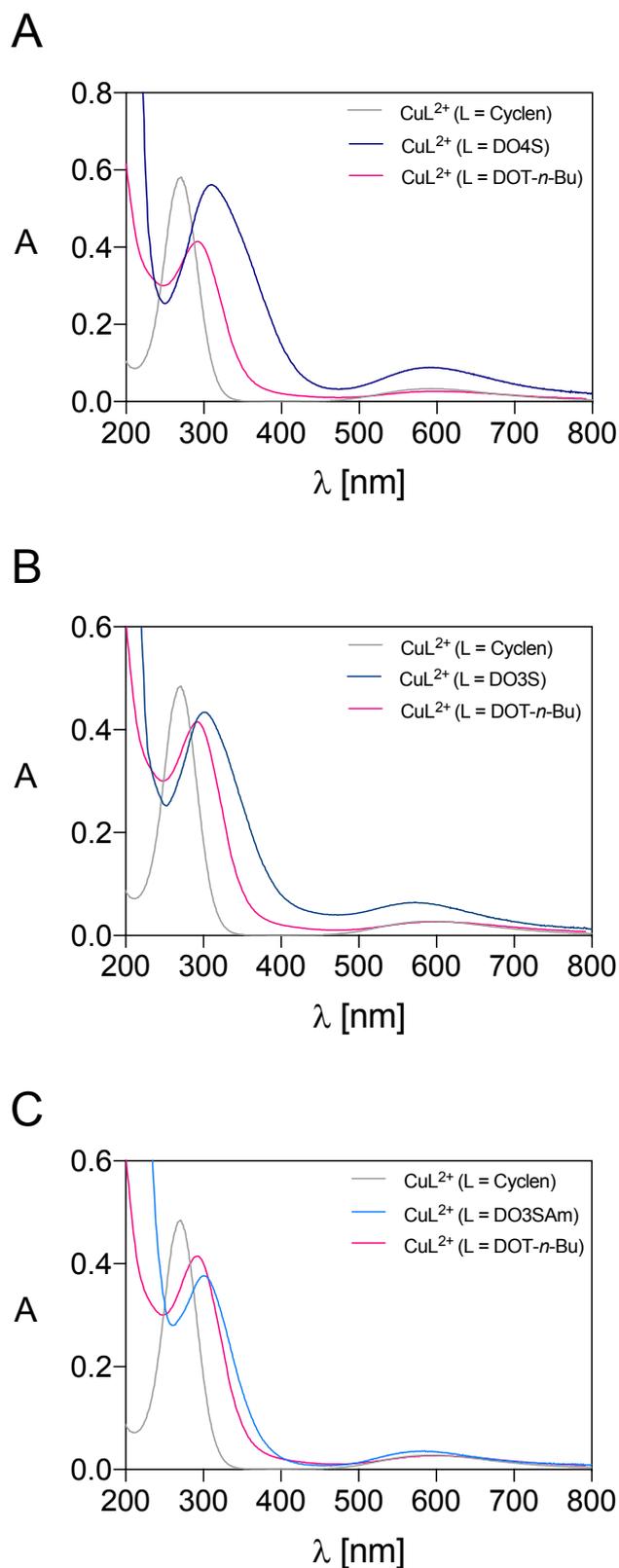
Figure S17. Comparison of the electronic spectra of the CuL^{2+} complexes formed by (A) DO4S, (B) DO3S and (C) DO3SAm (data from **Figure S8**) with those of the same complex formed by cyclen ($C_{Cu^{2+}} = C_{cyclen} = 1.5 \cdot 10^{-4}$ mol/L) and by DOT-*n*-Bu ($C_{Cu^{2+}} = C_{DOT-n-tBu} = 2.1 \cdot 10^{-4}$ mol/L). The Cu^{2+}-cyclen spectra obtained in this work agree with the literature data.[5,6]
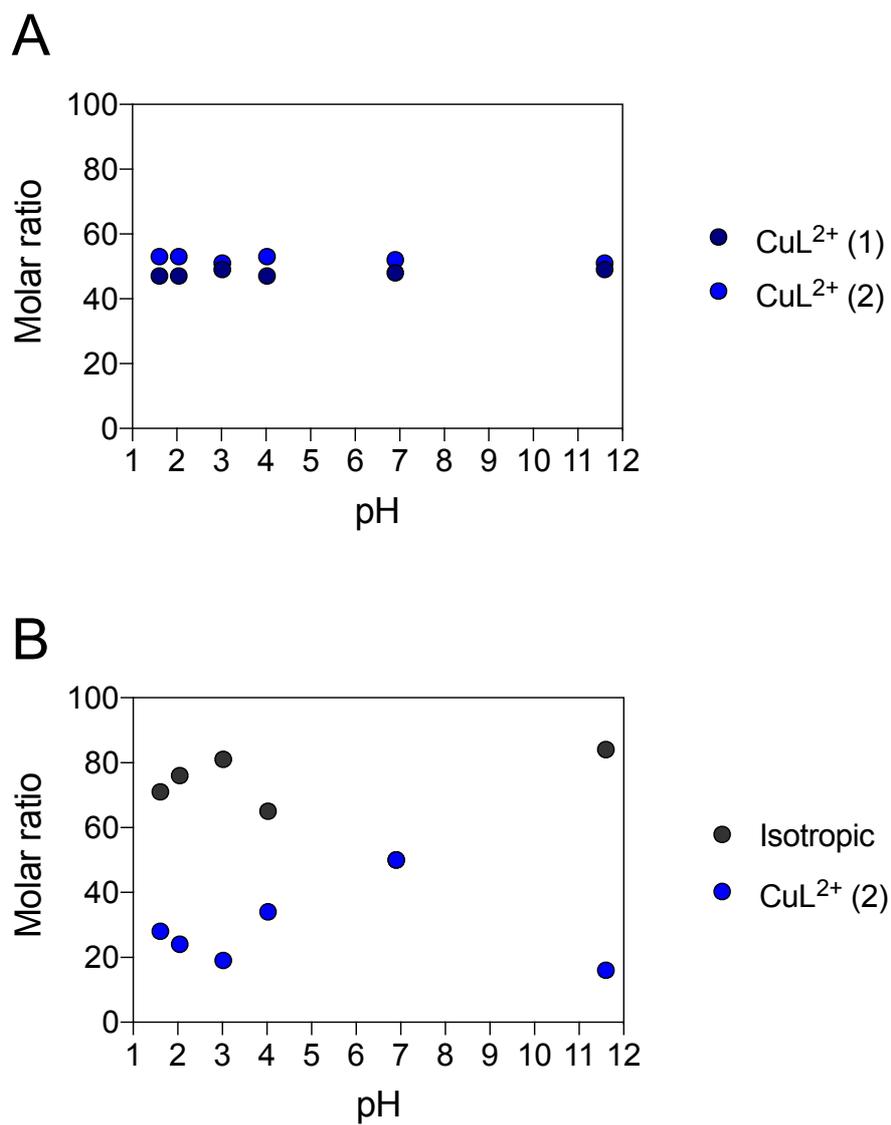
Figure S18. Component ratios obtained from the simulation of Cu^{2+}-DO4S EPR spectra recorded at (A) room temperature and (B) 77 K.
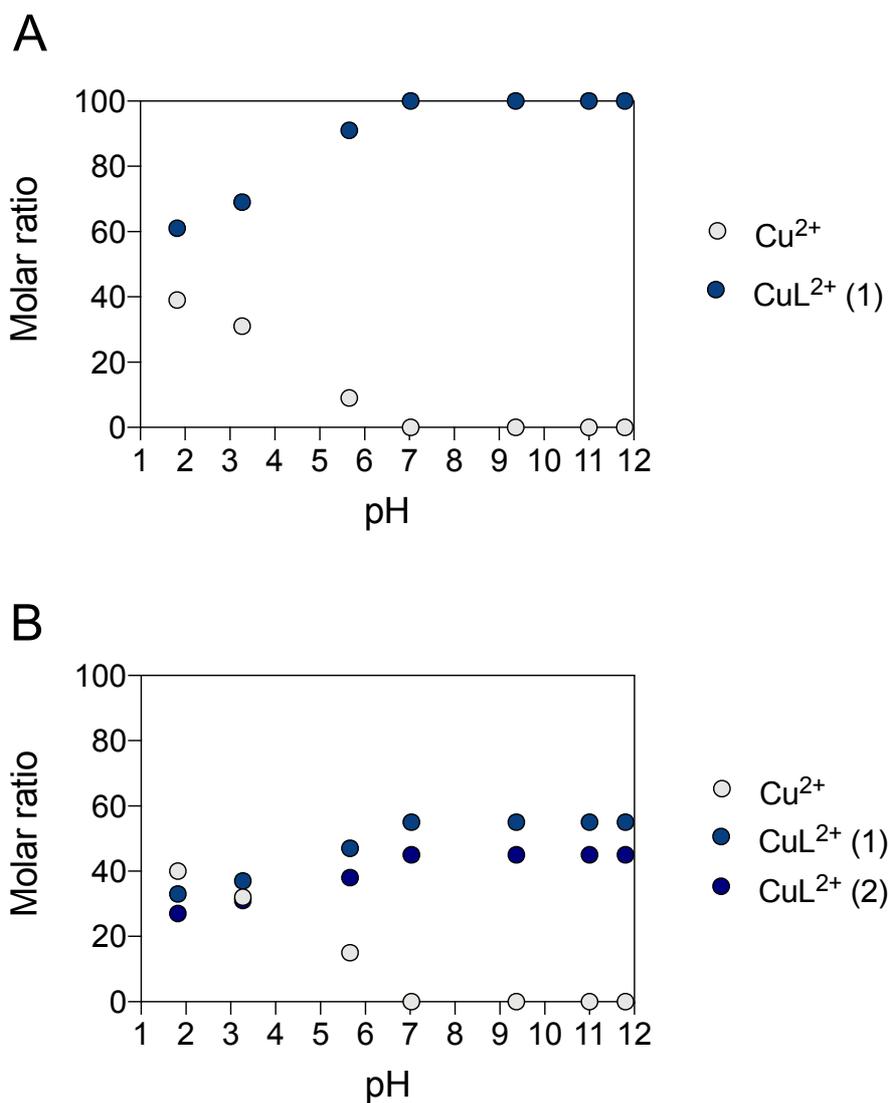
Figure S19. Component ratios obtained from the simulation of Cu^{2+}-DO3S EPR spectra recorded at (A) room temperature and (B) 77 K.

[4N]   [4N,S]   [4N,2S]
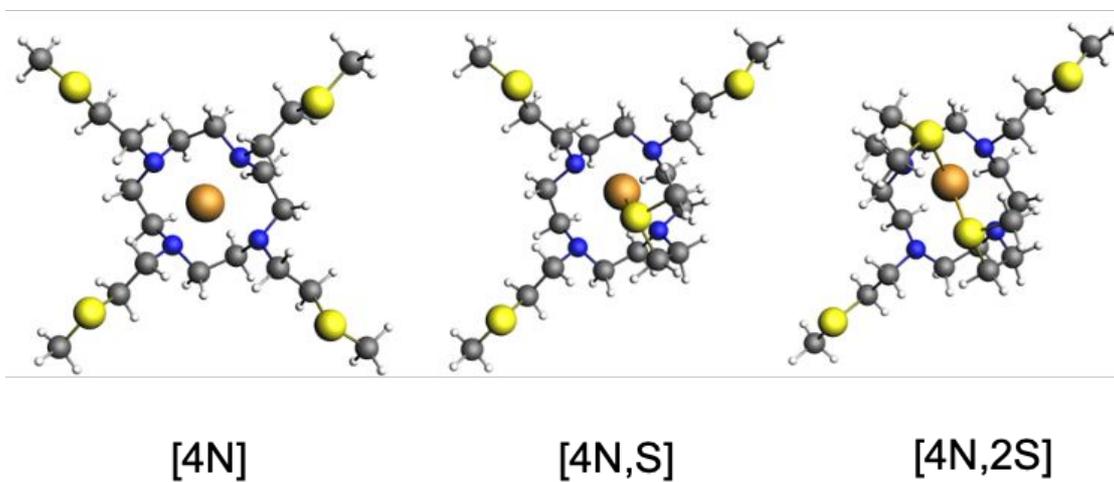
Figure S20. DFT-examined isomers of the CuL^{2+} complex formed by DO4S.
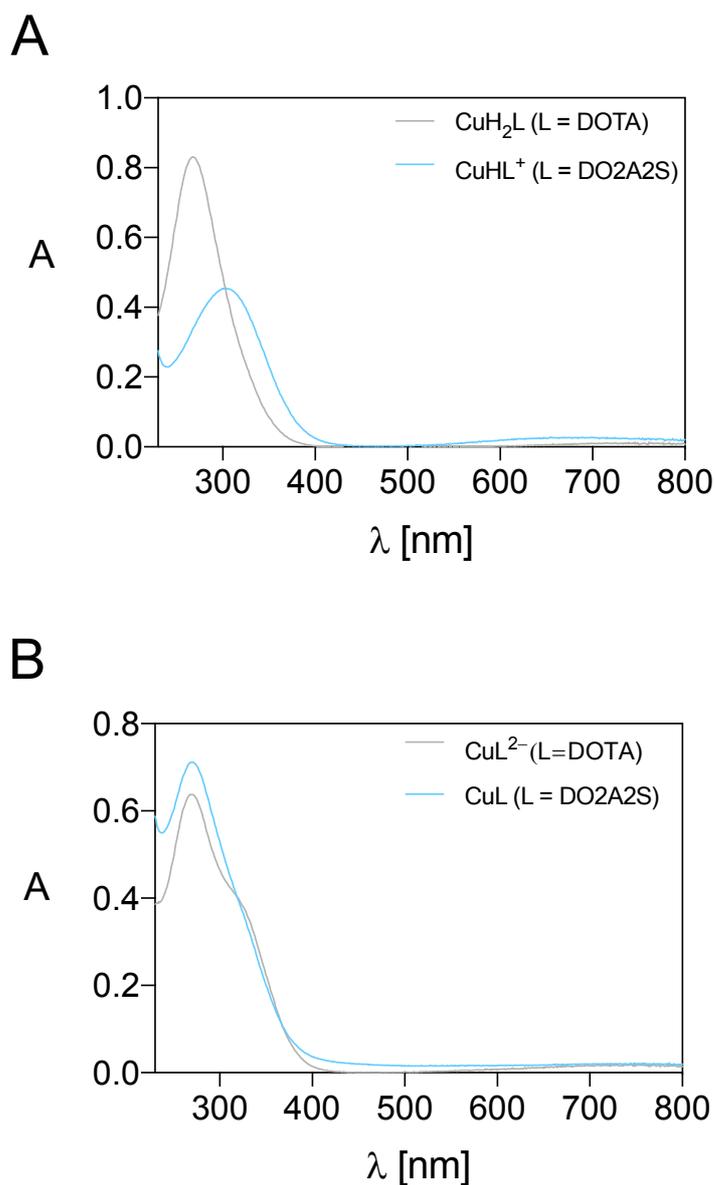
Figure S21. Comparison of the UV-Vis spectra of (A) CuHL$^+$ for DO2A2S (data from **Figure 2**) and CuH$_2$L for DOTA ($C_{Cu^{2+}} = C_{DOTA} = 2.0 \cdot 10^{-4}$ mol/L); (B) CuL for DO2A2S (data from **Figure S8**) and CuL^{2-} for DOTA ($C_{Cu^{2+}} = C_{DOTA} = 2.0 \cdot 10^{-4}$ mol/L). The Cu^{2+}-DOTA spectra obtained in this work agree with the literature data.[7]
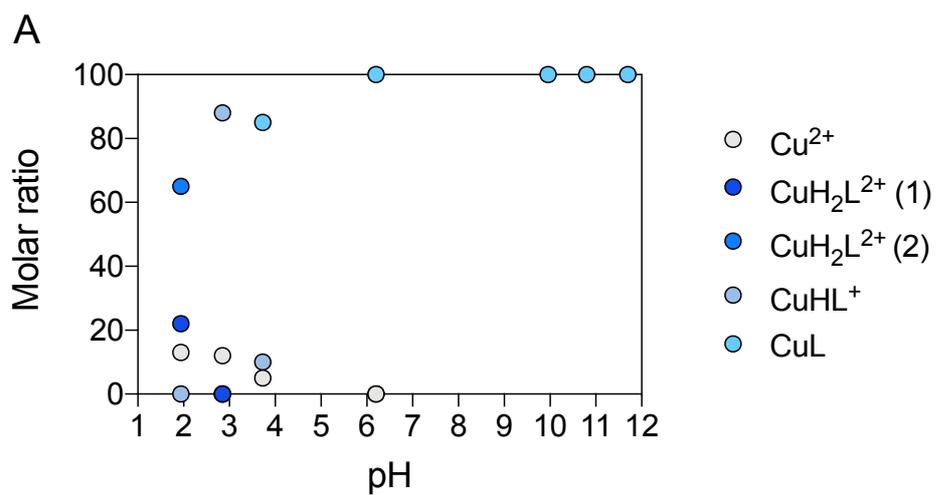
Figure S22. Component ratios obtained from the simulation of Cu^{2+}-DO2A2S EPR spectra recorded at 77 K.
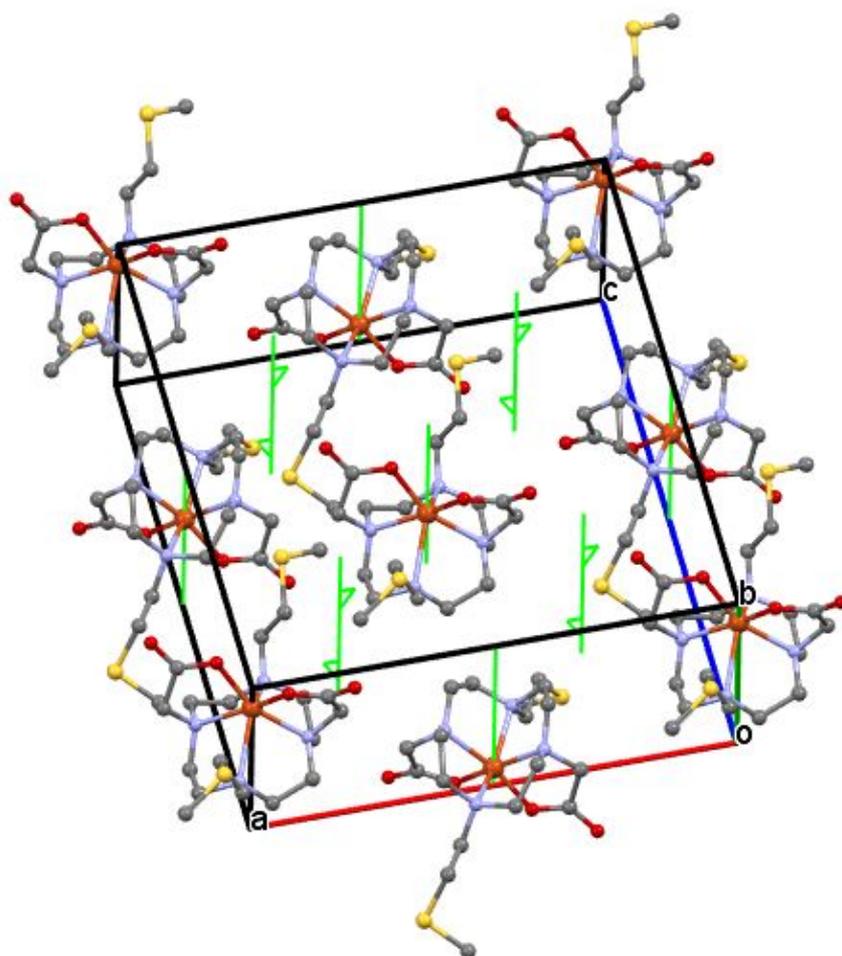
Figure S23. Unit cell of crystal [Cu(DO2A2S)] showing the 2-fold rotation and screw axes.
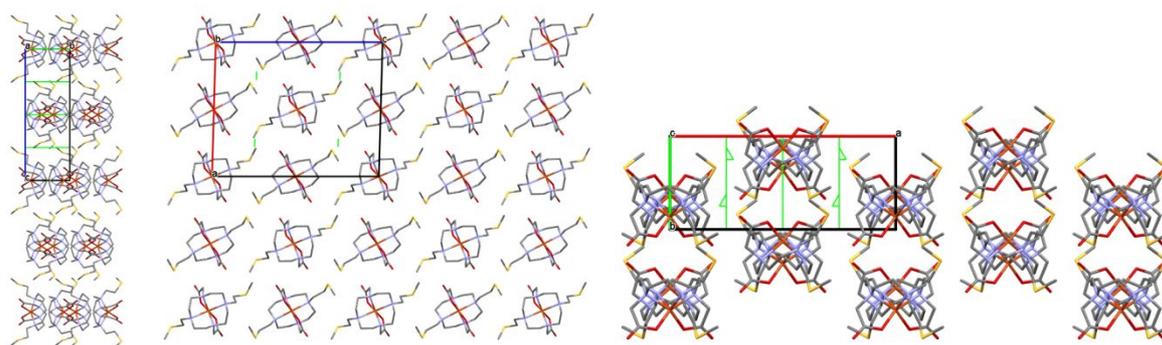
Figure S24. Packing arrangements in crystal [Cu(DO2A2S)] viewed from the crystallographic directions 'a', 'b' and 'c'.
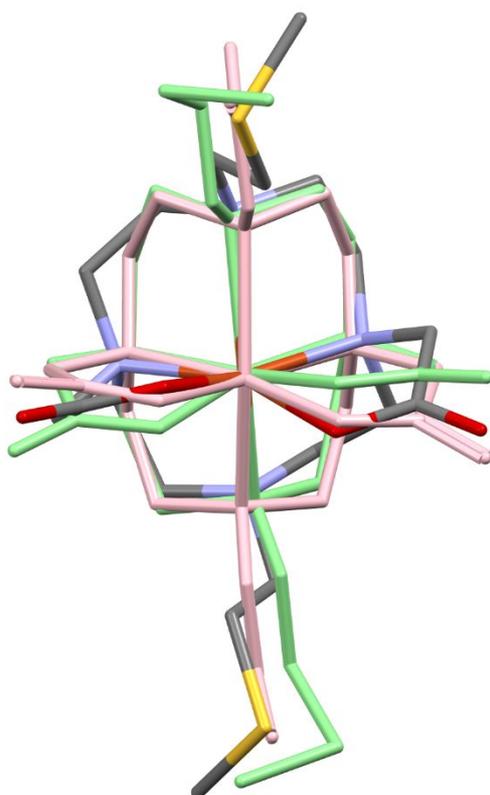

Figure S25. Comparison of the conformation of molecules in the asymmetrical unit of crystal [Cu(DO2A2S)] by overlay of the two molecules (molecule #1 is coloured by element, and #2 is green) together with crystal structure of Cu-DOTA (pink, Ref. Code FEKVAS).[8]
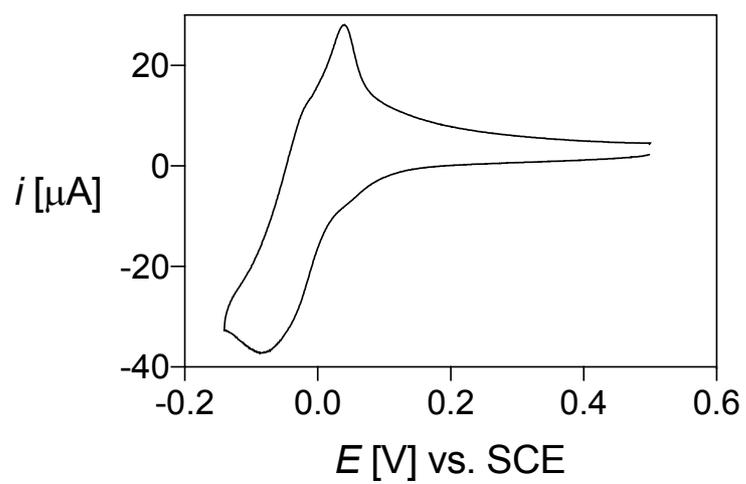
Figure S26. Cyclic voltammogram of unbound Cu^{2+} ($C_{Cu^{2+}}$ = 2.3·10^{-3} mol/L) in aqueous solution at pH 7, I = 0.15 mol/L $NaNO_3$ and T = 25 °C, acquired at a scan rate of 0.1 V/s.

A

B

C
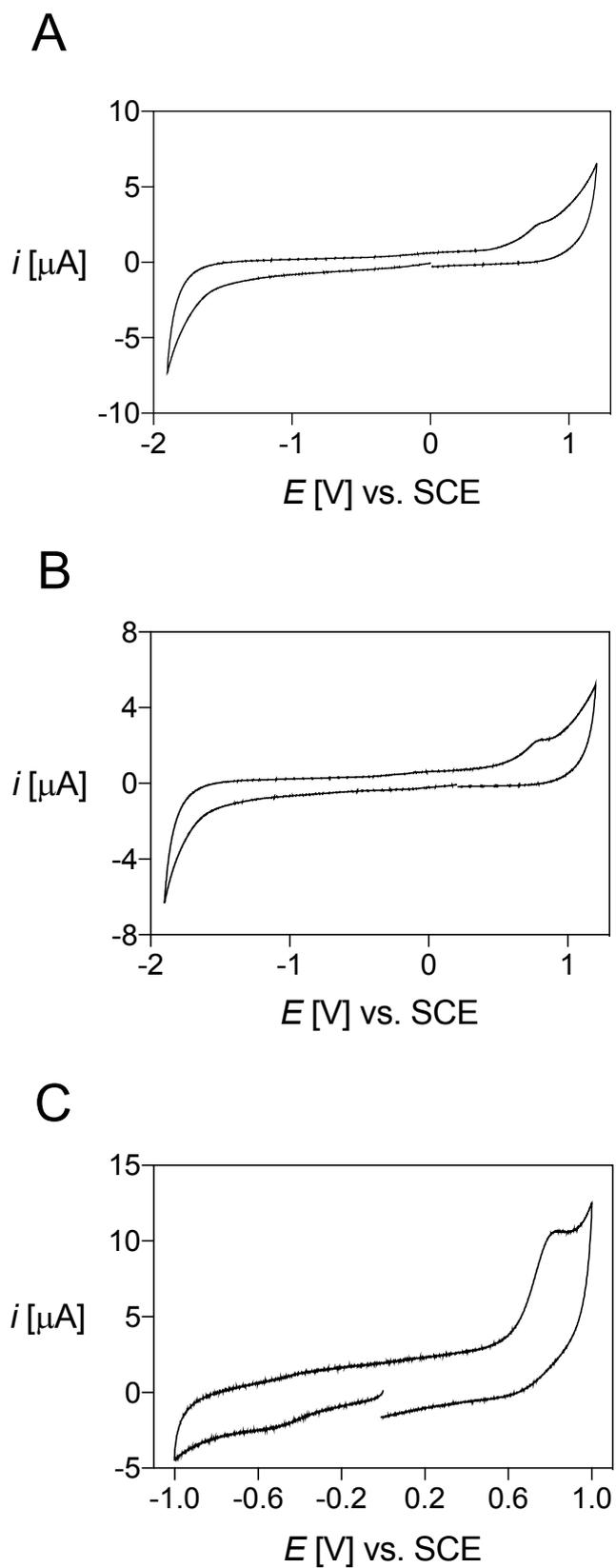
Figure S27. Cyclic voltammogram of (A) DO4S (C_{DO4S} = 1.0·10^{-3} mol/L), (B) DO3S (C_{DO3S} = 1.1·10^{-3} mol/L) and (C) DO2A2S (C_{DO2A2S} = 1.0·10^{-3} mol/L) in aqueous solution at pH 7, I = 0.15 mol/L NaNO$_3$ and T = 25 °C, acquired at a scan rate of 0.1 V/s.
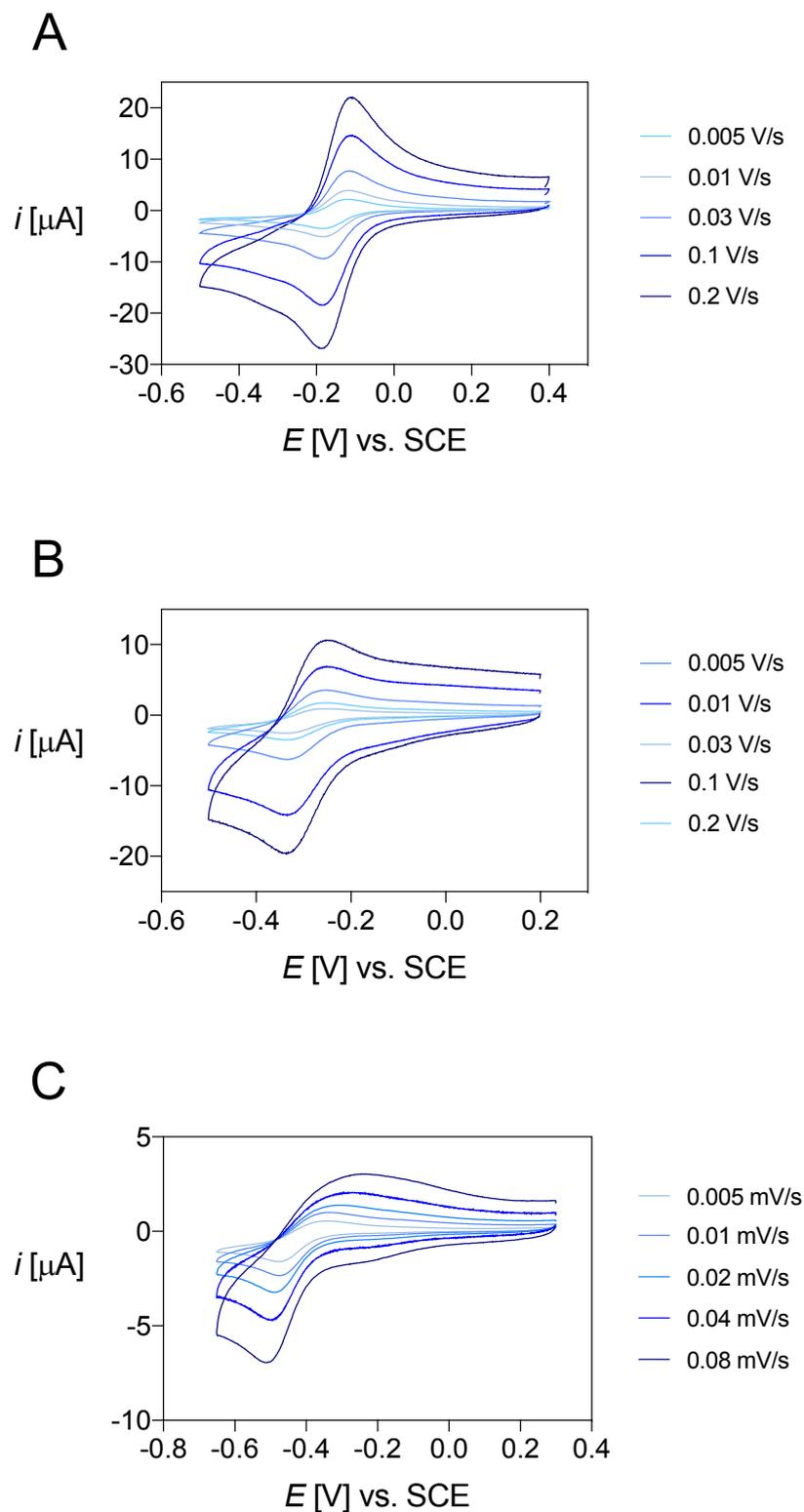
**Figure S28.** Cyclic voltammograms of copper complexes of (A) DO4S ($C_{CuL^{2+}}$ = 1.0·10⁻³ mol/L), (B) DO3S ($C_{CuL^{2+}}$ = 1.1·10⁻³ mol/L) and (C) DO2A2S ($C_{CuL^{2+}}$ = 6.48·10⁻⁴ mol/L) in aqueous solution at pH 7, I = 0.15 mol/L NaNO₃ and T = 25 °C, acquired at different scan rates (0.005 - 0.2 V/s).
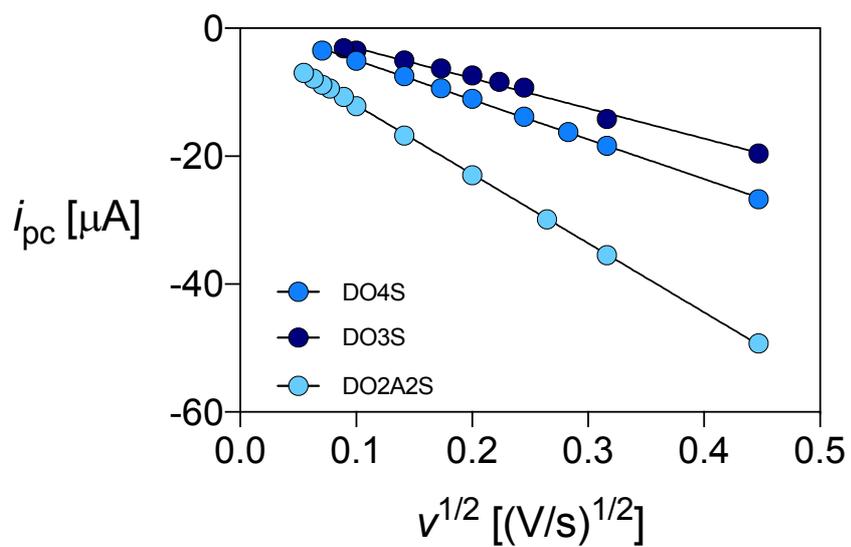
Figure S29. Variation of the cathodic current intensity (i_{pc}) with the square root of the scan speed ($v^{1/2}$) for the Cu^{2+} complexes of (A) DO4S, (B) DO3S and (C) DO2A2S, and linear regressions.
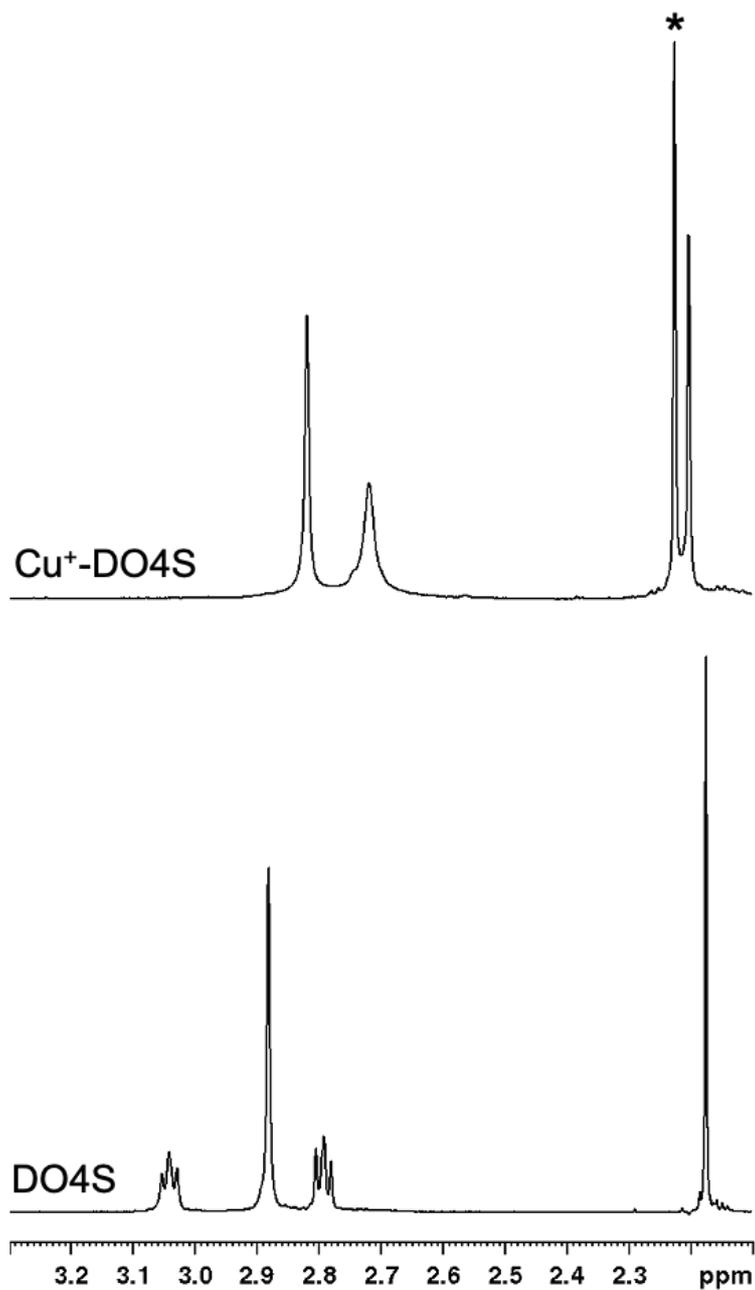
Figure S30. Comparison between the ^{1}H-NMR spectra of Cu^{+}-DO4S (400 MHz, RT, H_2O + 10% D_2O) at pH 7 (data from **Figure 9**) and free monoprotonated DO4S (600 MHz, RT, D_2O). Data for the latter were taken from our previous work.[1] The signal marked with an asterisk (2.22 ppm) is related to acetone impurity.
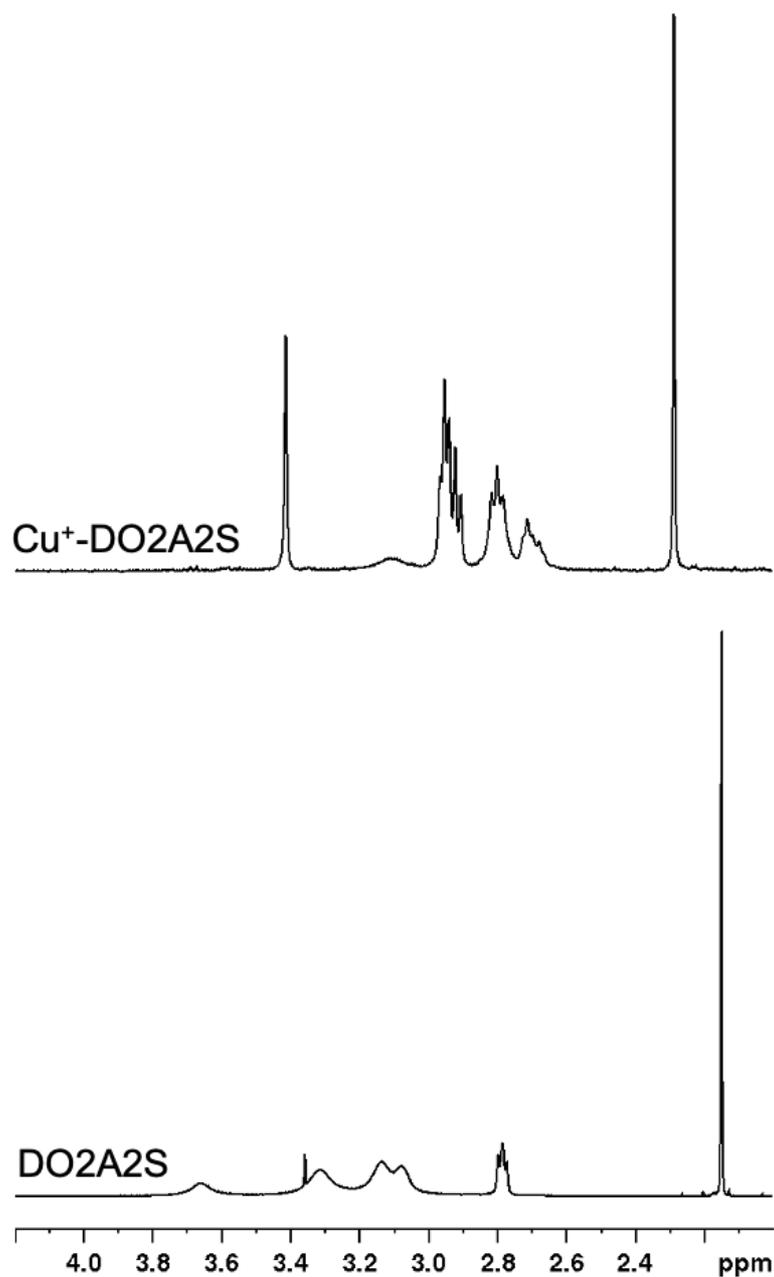
Figure S31. Comparison between the ^{1}H-NMR spectra of Cu$^+$-DO2A2S (400 MHz, RT, H$_2$O + 10% D$_2$O) at pH 7 (data from **Figure 9**) and free monoprotonated DO2A2S (600 MHz, RT, D$_2$O). Data for the latter were taken from our previous work.[1]
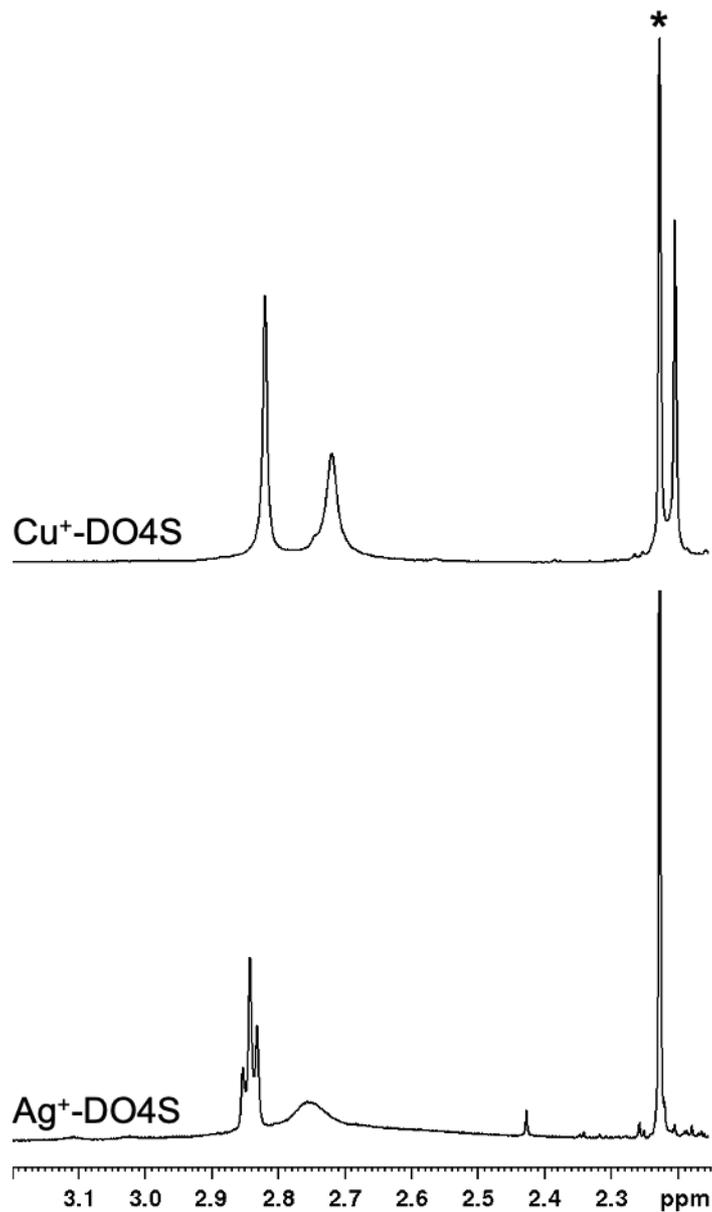
Figure S32. Comparison between the ^{1}H-NMR spectra of Cu^{+}-DO4S (400 MHz, RT, H_2O + 10% D_2O) (data from **Figure 9**) and of Ag^{+}-DO4S solutions (600 MHz, RT, D_2O) at pH 7. Data for the latter were taken from our previous work.[9] The signal marked with an asterisk (2.22 ppm) is related to acetone impurity.

LUMO_M   **HOMO-3**
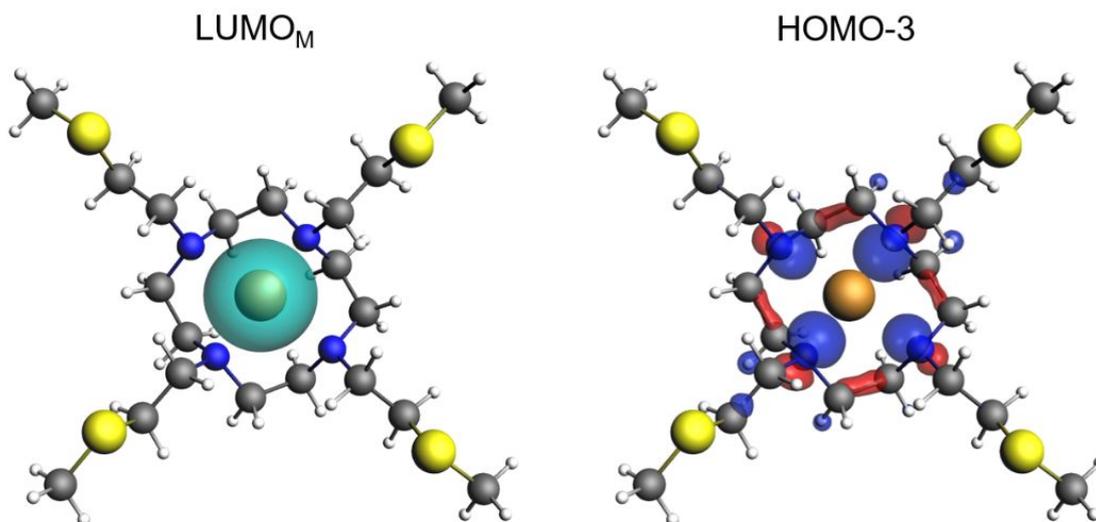
Figure S33. Main interacting symmetry-adapted fragment orbitals (SFOs) of the Cu$^+$-DO4S complex displaying a [4N] coordination mode.
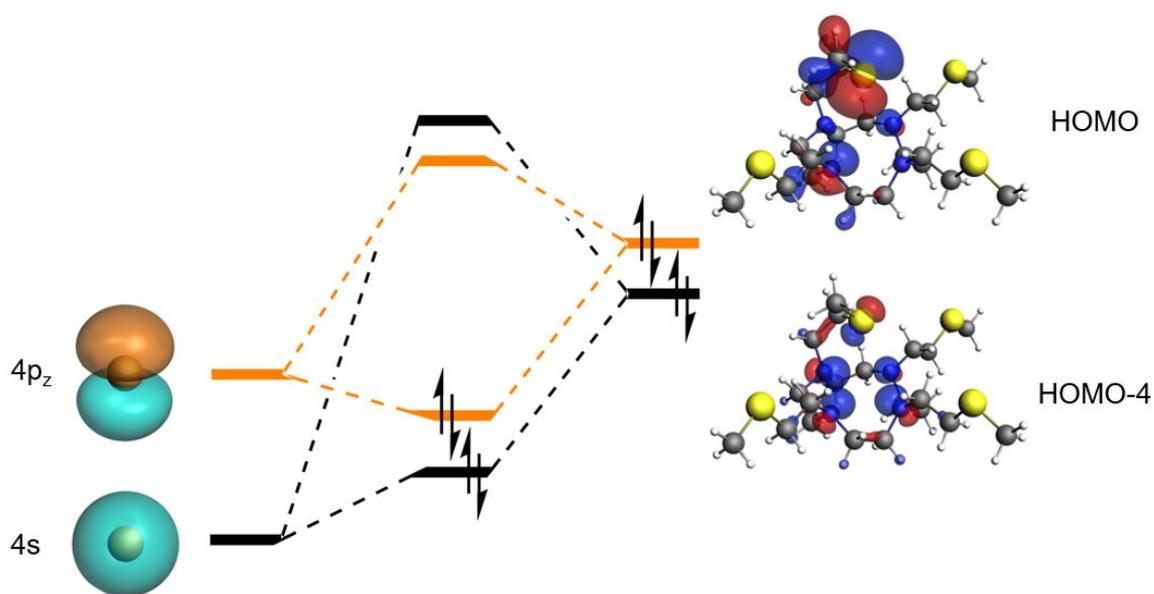
Figure S34. Molecular orbital diagram showing the two main bonding mode of the Cu$^+$-DO4S complex displaying a [4N,S] coordination mode. On the left, symmetry-adapted fragment orbitals (SFOs) representing the $4s$ and the $4p_z$ orbitals located on the metal center. On the right, ligand SFOs involved in the primary (black) and secondary (orange) molecular bonding and antibonding orbital.
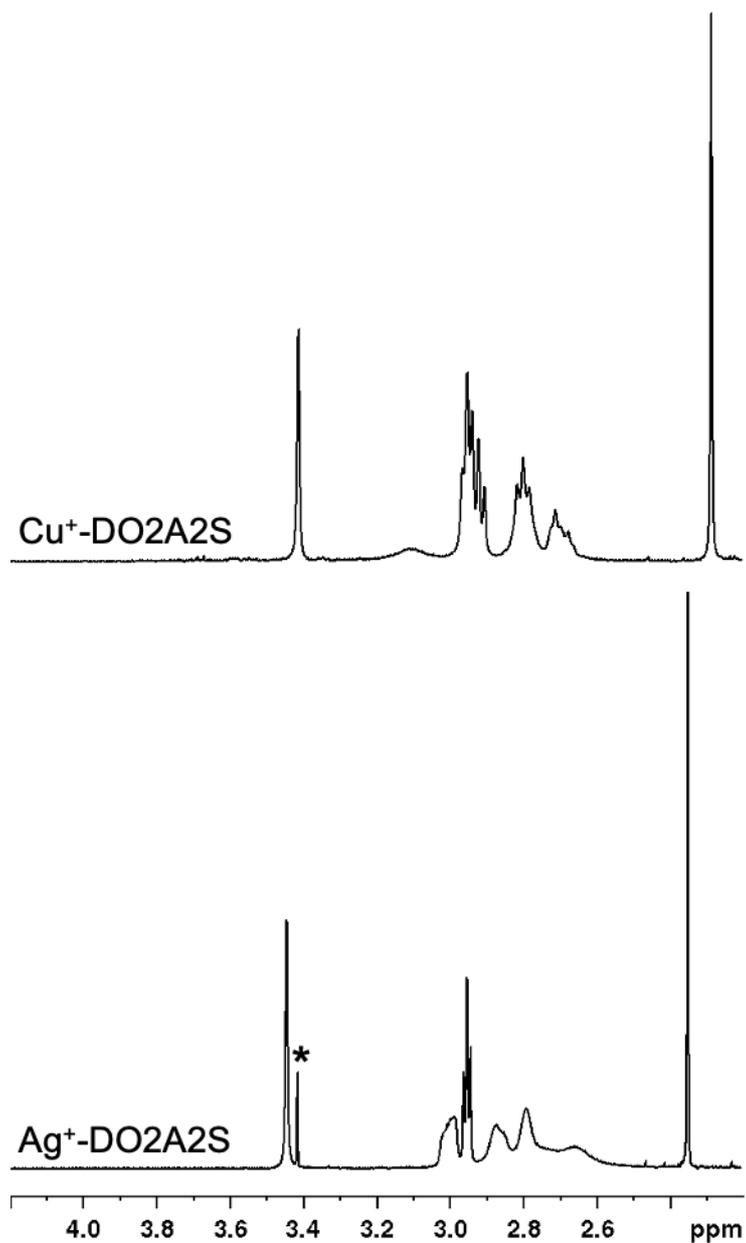
Figure S35. Comparison between the ¹H-NMR spectra of Cu⁺-DO2A2S (400 MHz, RT, H_2O + 10% D_2O) (data from **Figure 9**) and Ag⁺-DO2A2S (600 MHz, RT, D_2O) at pH 7. Data for the latter were taken from our previous work.[9] The signal marked with an asterisk is related to methanol impurity.

Determination of the stability constants of the Cu⁺ complexes from voltammetric data

The relationship between the stability constants of the Cu^{2+} and Cu^+ complexes with the ligand L was obtained using the following thermodynamic cycle:

1) Cu^{2+} + L $\rightleftharpoons$ CuL^{2+} $\qquad$ ΔG_1^0 = $-RT \ln(\beta_{II})$

2) CuL^{2+} + e⁻ $\rightleftharpoons$ CuL^+ $\qquad$ ΔG_2^0 = $-nF E_2^0$

3) Cu^{2+} + e⁻ $\rightleftharpoons$ Cu^+ $\qquad$ ΔG_3^0 = $-nF E_3^0$

4) Cu^+ + L $\rightleftharpoons$ CuL^+ $\qquad$ ΔG_4^0 = $-RT \ln(\beta_I)$
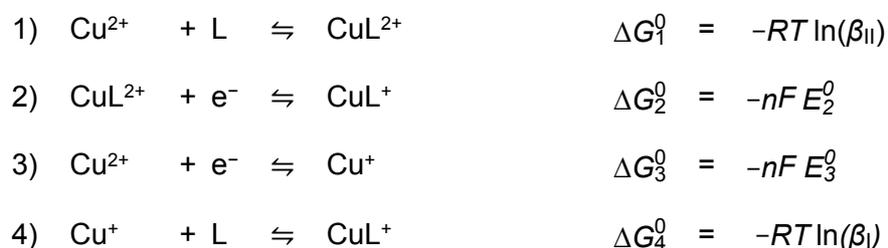
where $n = 1$, β_{II} and β_I represent the formation constants of CuL^{2+} and CuL^+, respectively, and $E°_2$ is the standard potential for the unbound Cu^{2+}/Cu^+ redox couple. It was assumed that the experimental $E_{1/2}$ values approximate the standard potentials ($E°_3$).
The stability constants for the Cu^+ complexes were obtained from:

$$\Delta G_4^0 = \Delta G_1^0 + \Delta G_2^0 - \Delta G_3^0 \qquad (6)$$

so that:

$$\ln(\beta_I) = \ln(\beta_{II}) + \frac{nF}{RT}(E_2^0 - E_3^0) \qquad (7)$$

Supplementary referennces

(1)   Tosato, M.; Verona, M.; Doro, R.; Dalla Tiezza, M.; Orian, L.; Andrighetto, A.; Pastore, P.; Marzaro, G.; Di Marco, V. Toward Novel Sulphur-Containing Derivatives of Tetraazacyclododecane: Synthesis, Acid–Base Properties, Spectroscopic Characterization, DFT Calculations, and Cadmium(II) Complex Formation in Aqueous Solution. *New J. Chem.* **2020**, *44* (20), 8337–8350.

(2)   Pniok, M.; Kubíček, V.; Havlíčková, J.; Kotek, J.; Sabatie-Gogovà, A.; Plutnar, J.; Huclier-Markai, S.; Hermann, P. Thermodynamic and Kinetic Study of Scandium(III) Complexes of DTPA and DOTA: A Step Toward Scandium Radiopharmaceuticals. *Chem. Eur. J.* **2014**, *20* (26), 7944–7955.

(3)   Di Marco, V.; Pastore, P.; Tosato, M.; Andrighetto, A.; Borgna, F.; Realdon, N. pH-Static Titrations for Kinetic Studies of Metal-Ligand Complex Formation: The Case Example of the Reaction between Strontium(II) and DOTA. *Inorganica Chim. Acta* **2019**, *498*, 119147.

(4)   Leugger, A. P.; Hertli, L.; Kaden, T. A. Metal Complexes with Macrocyclic Ligands. Ring Size Effect on the Complexation Rates with Transition Metal Ions. *Helv. Chim. Acta* **1978**, *61* (7), 2296.

(5)   Styka, M. C.; Smierciak, R. C.; Blinn, E. L.; DeSimone, R. E.; Passariello, J. V. Copper(II) Complexes Containing a 12-Membered Macrocyclic Ligand. *Inorg. Chem.* **1978**, *17* (1), 82–86.

(6)   Lacerda, S.; Campello, M. P.; Santos, I. C.; Santos, I.; Delgado, R. Study of the Cyclen Derivative 2-[1,4,7,10-Tetraazacyclododecan-1-yl]-Ethanethiol and Its Complexation Behaviour towards d-Transition Metal Ions. *Polyhedron* **2007**, *26* (14), 3763–3773.

(7)   Ševčik, R.; Vanek, J.; Lubal, P.; Kotková, Z.; Kotek, J.; Hermann, P. Formation and Dissociation Kinetics of Copper(II) Complexes with Tetraphosphorus Acid DOTA Analogs. *Polyhedron* **2014**, *67*, 449–455.

(8)   Riesen, A.; Zehnder, M.; Kaden, T. A. Metal Complexes of Macrocyclic Ligands. Part XXIII. Synthesis, Properties, and Structures of Mononuclear Complexes with 12- and 14-membered Tetraazamacrocycle-*N*,*N'*,*N''*,*N'''*-tetraacetic Acids. *Helv. Chim. Acta* **1986**, *69* (8), 2067–2073.

(9)   Tosato, M.; Asti, M.; Dalla Tiezza, M.; Orian, L.; Häussinger, D.; Vogel, R.; Köster, U.; Jensen, M.; Andrighetto, A.; Pastore, P.; Di Marco, V. Highly Stable Silver(I) Complexes with Cyclen-Based Ligands Bearing Sulfide Arms: A Step Toward Silver-111 Labeled Radiopharmaceuticals. *Inorg. Chem.* **2020**, *59* (15), 10907–10919.